Tectonophysics 659 (2015) 122–136

Contents lists available at ScienceDirect

Tectonophysics

journal homepage: www.elsevier.com/locate/tecto

The Permian Dongfanghong island-arc gabbro of the Wandashan Orogen, NE China: Implications for Paleo-Pacific subduction

Ming-Dao Sun [a,b,c,*], Yi-Gang Xu [a], Simon A. Wilde [b], Han-Lin Chen [c], Shu-Feng Yang [c]

[a] State Key Laboratory of Isotope Geochemistry, Guangzhou Institute of Geochemistry, Chinese Academy of Sciences, Guangzhou 510640, China
[b] Department of Applied Geology, Curtin University, Perth, WA, 6845, Australia
[c] Department of Earth Science, Zhejiang University, Hangzhou, Zhejiang, China, 310027

ARTICLE INFO

Article history:
Received 9 March 2015
Received in revised form 7 July 2015
Accepted 27 July 2015
Available online 15 August 2015

Keywords:
Wandashan Orogen
Jiamusi Block
Sikhote-Alin accretionary complex
NE Asia
Paleo-Pacific

ABSTRACT

The Dongfanghong hornblende gabbro is located in the western part of the Wandashan Orogen and to the east of the Jiamusi Block in NE China. It was emplaced into Early Paleozoic oceanic crust (i.e. Dongfanghong ophiolite) at ~275 Ma and both later collided with the eastern margin of the Jiamusi Block. The Dongfanghong gabbro is subalkaline with high Na_2O contents and is characterized by enrichment in light rare earth elements (LREE), large ion lithosphile elements (LILE), Sr, Eu, and Ba, and depletion in high field strength elements (HFSE). The enriched isotopic signatures ($^{87}Sr/^{86}Sr_i$ = ~0.7065, $\varepsilon Nd(t)$ = ~−0.5, $^{208}Pb/^{204}Pb_i$ = ~38.05, $^{207}Pb/^{204}Pb_i$ = ~15.56, $^{206}Pb/^{204}Pb_i$ = ~18.20 and zircon $\varepsilon Hf(t)$ = ~+5.8) indicate an enriched mantle (EM2) source, with some addition of continental material. It has arc geochemical affinities similar to Permian arc igneous rocks in the eastern margin of the Jiamusi Block, the Yakuno Ophiolite in SW Japan, arc rocks along the western margin of the North America Craton, and also the Gympie Group in eastern Australia. All these features, together with information from tectonic discrimination diagrams, suggest that the Dongfanghong gabbro formed in an immature island arc. The spatial configuration of ~290 Ma immature continental arc rocks in the eastern part of the Jiamusi Block and the ~275 Ma immature island arc Dongfanghong gabbro in the Wandashan Orogen to the east is best explained by eastward arc retreat and slab roll-back of the Paleo-Pacific Plate. This model is also supported by the Carboniferous–Permian stratigraphic transition in the Jiamusi Block from oceanic carbonate rocks to coal-bearing terrestrial clastic rocks and andesites. We thus suggest that both Paleo-Pacific subduction and roll-back occurred in the Early Permian along the eastern margin of Asia.

1. Introduction

Widespread igneous rocks and terrestrial sedimentary basins formed in the eastern Central Asian Orogenic Belt (CAOB), the North China Craton, and the South China Block during the Permian (Jahn, 2004, 2010; Li and Li, 2007; Windley et al., 2007; Yang et al., 2010; Lehmann et al., 2010; Meng et al., 2011; Lv et al., 2011; Yu et al., 2013a). Most of these were intraplate/marginal continental geological events considered to result from subduction of the Mongol-Okhotsk Ocean, the Paleo-Asian Ocean, the Paleo-Tethys Ocean, and/or the Paleo-Pacific Ocean (Xiao et al., 2003; Li, 2006; Jian et al., 2010; Wu et al., 2011; Zhou et al., 2009; Zhou and Wilde, 2013; Donskaya et al., 2013; Wakita, 2013) (Fig. 1a). However, due to spatial and temporal overlap, it is difficult to determine which oceanic subduction was responsible for a given geological event. In South China, some researchers have applied the Paleo-Pacific subduction model to interpret intraplate/marginal continental magmatism and sedimentary events (Li and Li, 2007; Li et al., 2012a,b); whereas others prefer the Paleo-Tethys subduction model (Fan et al., 2010; Hennig et al., 2009; Jian et al., 2009; Zhong et al., 2013). In NE China, Permo-Triassic magmatism is generally interpreted to be the result of Paleo-Asian Ocean subduction and ultimate closure (Zhang et al., 2009; Xu et al., 2009; Liu et al., 2010a,b; Meng et al., 2011; Cao et al., 2012; Wang et al., 2015), but with some influence from Paleo-Pacific subduction (Wilde and Zhou, in press; Yang et al., 2015). In particular, there is controversy regarding the timing of initiation of Paleo-Pacific subduction towards East Asia, for example: from the Permian (Li and Li, 2007; Li et al., 2012a,b), the Triassic (Zhou et al., 2014), the Jurassic (Wang et al., 2015; Zhou et al., 2006), or the Cretaceous (Chen et al., 2008). Therefore, it is important to investigate and identify the earliest arc rocks related to Paleo-Pacific subduction along the Pacific margin of East Asia.

In this study, we report SHRIMP U–Pb zircon geochronological, whole-rock geochemical and Sr–Nd–Pb and zircon Hf isotopic results for the Dongfanghong gabbro in the Wandashan Orogen, NE China, and compare these with Permian island arc rocks of the circum-Paleo-Pacific Ocean. Our results and conclusions contribute to understanding the early evolution of Paleo-Pacific subduction beneath East Asia.

* Corresponding author at: 511 Kehua St, Wushan, Tianhe district, Guangzhou 510640, China.
E-mail address: smd@zju.edu.cn (M.-D. Sun).

http://dx.doi.org/10.1016/j.tecto.2015.07.034
0040-1951/

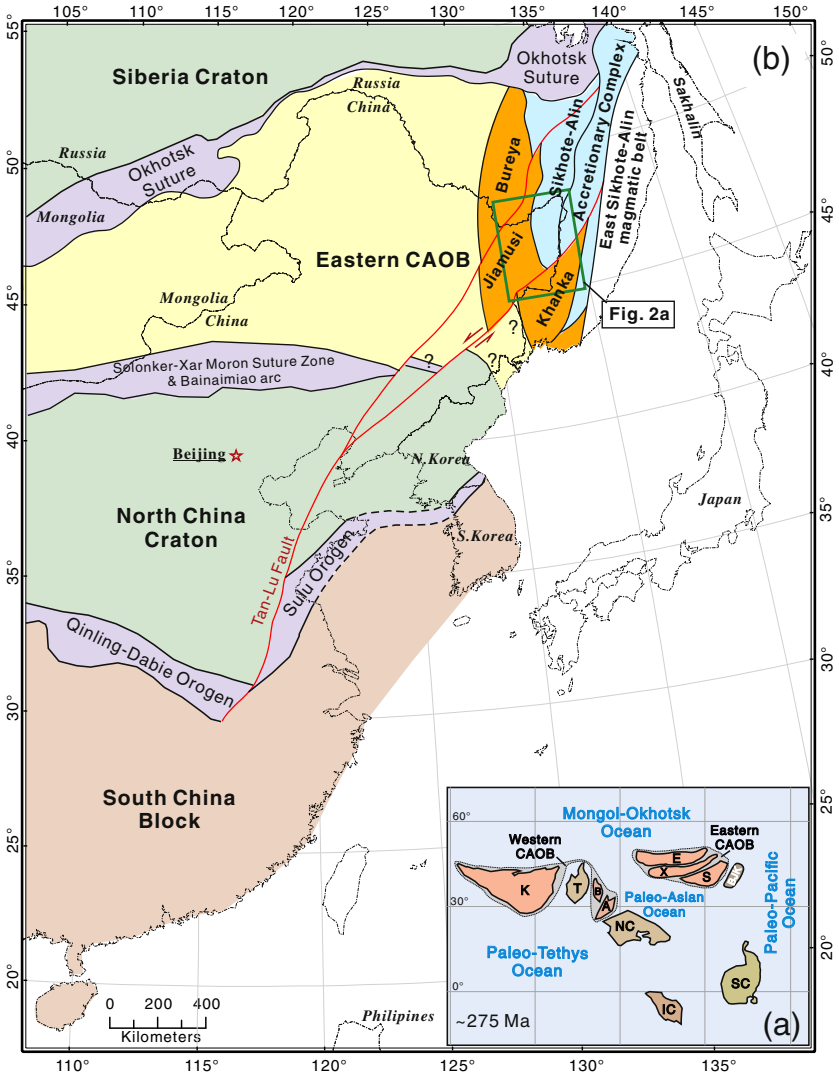

Fig. 1. (a) Simplified tectonic sketch map of East Asia in the Permian (after Xiao et al., 2003; Li, 2006; Jian et al., 2010; Wu et al., 2011; Zhou et al., 2009; Zhou and Wilde, 2013; Zhong et al., 2013; Xiao et al., 2015). BJK: Bureya-Jiamusi Khanka Block; NC: North China Craton; T- Tarim Craton; IC: Indochina Block; Eastern CAOB (Central Asian Orogenic Belt) includes the E—Erguna, X—Xing'an, and S—Songliao blocks; Western CAOB includes the K—Kazakhstan collage system, B—Beishan, and A—Alxa blocks. (b) Tectonic sketch map of present-day East Asia (after Sun et al., 2015). Eastern CAOB (Central Asian Orogenic Belt) includes the Erguna, Xing'an, and Songliao blocks.

2. Geological setting

The Wandashan Orogen, also known as the Nadanhada Terrane (Li et al., 1979; Mizutani et al., 1990; Shao et al., 1992; Sun et al., 2015), is located in NE China. It is the Chinese part of the circum-Pacific Sikhote-Alin accretionary complex that is best developed in Far East Russia (Kemkin, 2012; Mizutani and Kojima, 1992). Tectonically, the Wandashan Orogen is located between the Bureya–Jiamusi–Khanka Block to the west (Sorokin et al., 2010; Wilde et al., 1999, 2000; Wu et al., 2001; Zhou and Wilde, 2013; Zhou et al., 2009, 2010) and the Cretaceous to Early Paleogene continental arc of the East Sikhote-Alin magmatic belt at the east (Grebennikov and Popov, 2014) (Fig. 1b).

The Wandashan Orogen consists of two major components: the Paleozoic to Early Mesozoic Yuejinshan Complex in the west and the Late Mesozoic Raohe Complex in the east (Zhou et al., 2014) (Fig. 2). The boundary between the two complexes is not clear in the field due to poor exposure.

The Yuejinshan Complex is composed of a metamorphic mélange in the west, with ultramafic–mafic rocks in the east. The mélange consists of upper greenschist facies mica-schist, phengite-schist, quartz-schist, marble, and meta-mafic and ultramafic igneous rocks. The ultramafic–mafic rock association in the east is named the Dongfanghong Ophiolite. It consists of oceanic meta-ultramafic–mafic volcanic and intrusive rocks, including meta-peridotite, pyroxenite, (layered) gabbro, diorite and basalt. The architecture, geochronology, geochemistry and tectonic evolution of the Dongfanghong Ophiolite is still controversial. Zhang et al. (1997) and Zhou et al. (2014) also reported MORB-type metabasalt from the Yuejinshan Complex.

The Raohe Complex consists of accreted mid-Triassic to mid-Jurassic radiolarian chert and ultramafic–mafic rocks, and also Late Jurassic to Early Cretaceous trench-slope terrestrial-sourced clastic rocks. The similarity of radiolarian chert species indicates that the Raohe Complex is comparable to the Mino Complex in Japan (Mizutani and Kojima, 1992). The ultramafic–mafic volcanic and intrusive rocks, from bottom to top, consist of peridotite, pyroxenite, gabbro, and pillow basalt, all showing OIB-type geochemical and isotopic signatures. They have been recognized as fragments of oceanic islands and are well exposed in the Dadingzishan area (Cheng et al., 2006; Guo et al., 2010; Zhou et al., 2014).

3. Sample location and petrology

The Dongfanghong gabbro is an intrusive component of the Dongfanghong Ophiolite of the Yuejinshan Complex (HBGMR, 1987) (Fig. 2b). It crops out over a length of 100 m from west to east, and

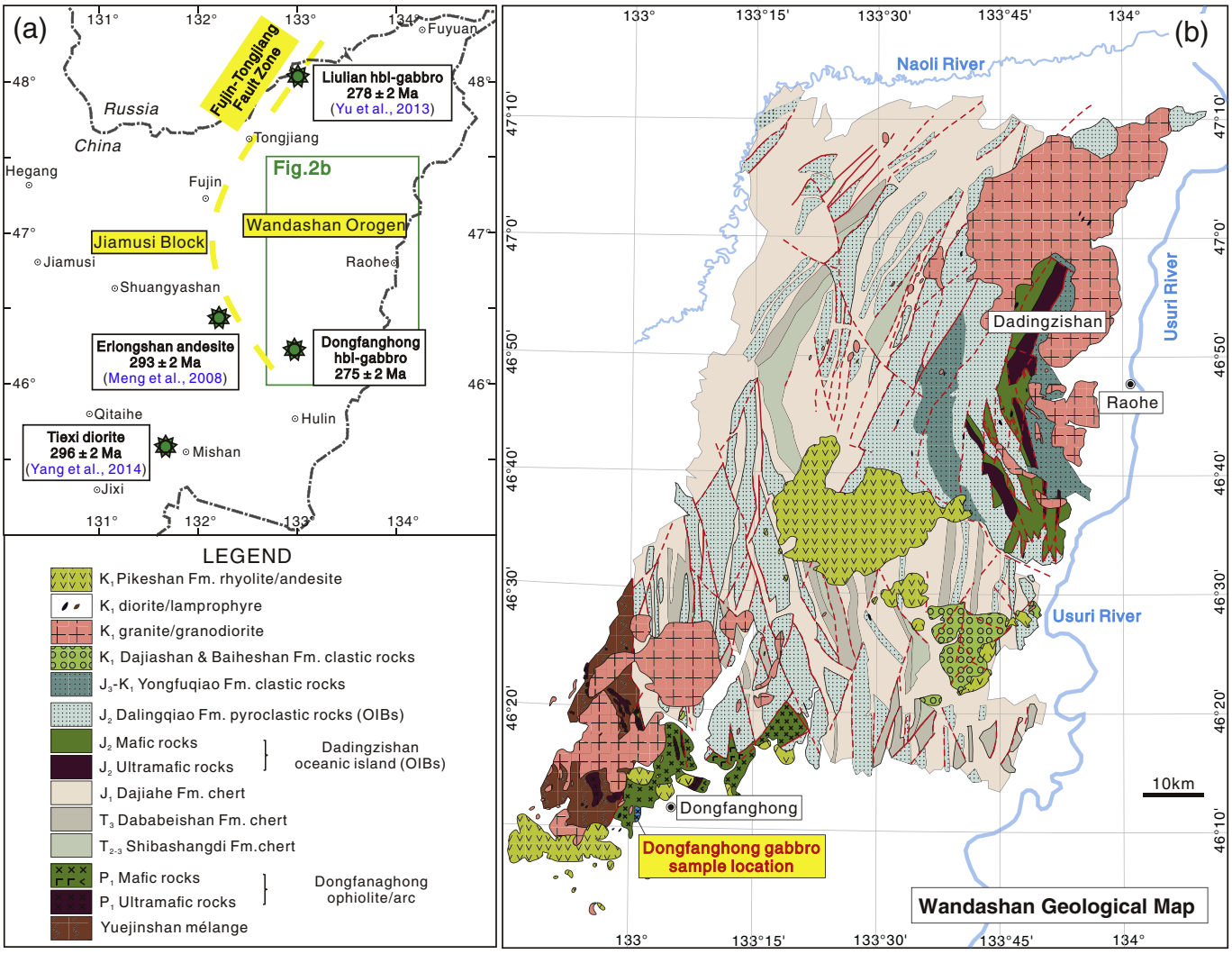

Fig. 2. (a) Sketch map of eastern Heilongjiang Province showing location of Permian igneous rocks (after Meng et al., 2008; Yu et al., 2013b; Yang et al., 2015). (b) Geological map of the Wandashan Orogen showing sample location (after HBGMR, 1987; Sun et al., 2015).

is located at 46°11′07″N, 133°01′07″E to the west-southwest of Dongfanghong Town (Fig. 2b). The gabbro is black and massive, but the contact relationship with the country-rock ophiolite is not exposed in this outcrop. Eleven samples were collected several meters apart along the outcrop. Three of them (RH02-8, 9, 10) contain abundant hornblende and were collected from the eastern portion of the outcrop. The remaining eight samples (RH02-1 to 5, 11 to 13) have abundant plagioclase and were collected from the western part of the outcrop.

The gabbro samples mainly consist of plagioclase, hornblende and clinopyroxene (Fig. 3). The plagioclase is euhedral and 2–5 mm in length. The clinopyroxene commonly occurs as relics, variably replaced by hornblende (Fig. 3b, c, e, f). Samples RH02-8, 9, 10 have clinopyroxene (15–20%), hornblende (15–30%), and plagioclase (50–65%). The other samples have clinopyroxene (10–15%), hornblende (10–15%), and plagioclase (65–75%).

4. Analytical methods

Approximately 10 kg of each of samples RH02-3 and RH02-10 was collected for zircon separation and geochemical analysis. Zircon grains were extracted by crushing and heavy liquid and magnetic separation at the Langfang Geological Services Corporation, Hebei Province, China, and about 100 grains from each sample were mounted, along with the Temora 2 zircon standard (Black et al., 2003). Cathodoluminescence (CL) images were taken using a Philips XL30 Scanning Electron Microscopy at Curtin University. SHRIMP U–Pb dating was performed using a SHRIMP II ion microprobe at Curtin University following standard procedures (Nelson et al., 1995). Six scans were run through the mass stations for data collection on each zircon. Standard BR266 (559 Ma, U = 909 ppm) (Stern, 2001) was used for U concentration and age calibration and Temora 2 (417 Ma) (Black et al., 2003) was used to monitor analytical conditions. Ages and concordia diagrams were calculated using the programs SQUID 1.03 (Ludwig, 2001) and ISOPLOT 3.0 (Ludwig, 2003).

100 g of each sample was crushed for geochemical analysis. Whole rock geochemical, zircon hafnium isotopic and Sr–Nd–Pb isotopic analyses were performed at the State Key Laboratory of Isotope Geochemistry, Guangzhou Institute of Geochemistry, Chinese Academy of Sciences. Major elements were analyzed using a Rigaku-100e X-ray fluorescence spectrometer (XRF). Trace and rare earth elements were analyzed using a Perkin Elmer Elan-6000 inductively-coupled plasma mass spectrometer (ICP-MS). The analytical precisions were 5–10% for REE, Rb, Sr, Cs, Ba, U, Th, Pb, Zr and Hf, and 20% for other trace elements. The Sr, Nd and Pb isotopes were analyzed using a Thermo-Finnigan Neptune MC-ICP-MS. The experimental procedures and the calculations of initial Sr, Nd, and Pb isotope ratios are the same as in Guo et al. (2010). Zircon hafnium isotopes were measured using a MC-ICP-MS equipped with a Geolas-193 nm laser ablation system. The Penglai

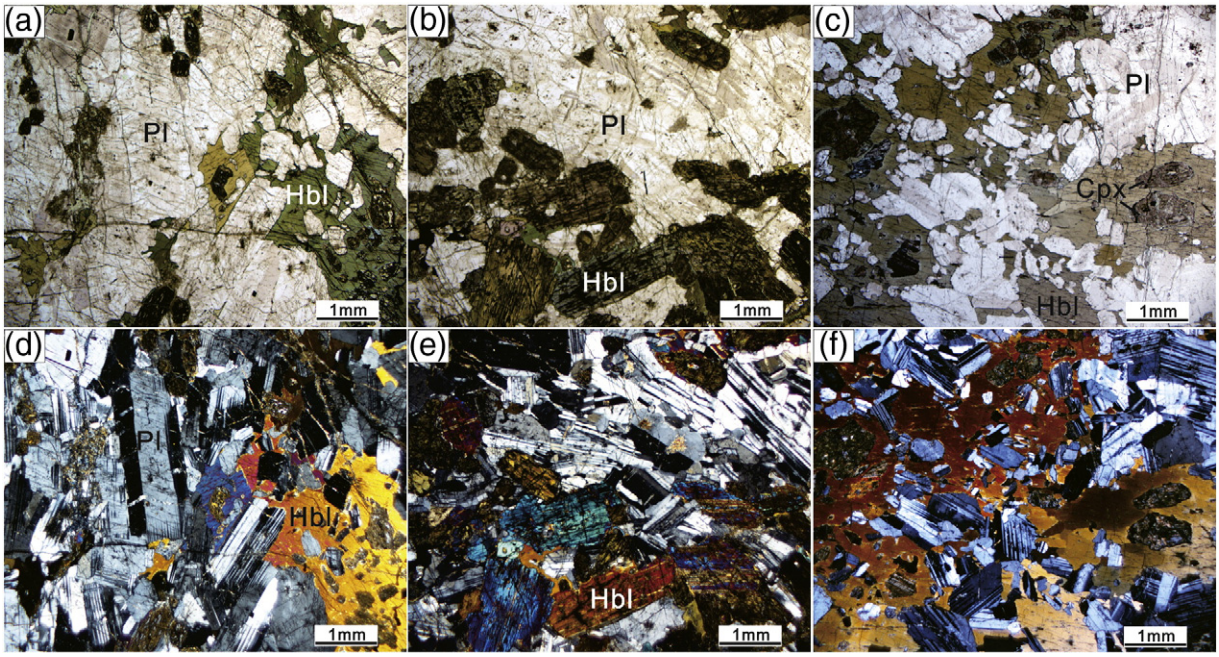

Fig. 3. Photomicrographs of gabbro samples RH02-3 (a, d) and RH02-10 (b, c, e, f). (a), (b), (c) are in plane-polarized light; (d), (e), (f) are in cross-polarized light. Cpx: clinopyroxene, Hbl: hornblende, Pl: plagioclase.

standard zircon was used for reference, with a recommended $^{176}Hf/^{177}Hf$ ratio of 0.282906 (Li et al., 2012b). The analyses were conducted on the same sites as the earlier SHRIMP U–Pb analyses. The $\varepsilon_{Hf}(t)$ values were calculated based on the decay constant for ^{176}Lu of 1.867×10^{-11}/year (Soderlund et al., 2004), and the present-day chondritic ratios of $^{176}Hf/^{177}Hf = 0.282785$ and $^{176}Lu/^{177}Hf = 0.0336$ (Bouvier et al., 2008).

5. Results

5.1. SHRIMP U–Pb zircon dating

The results of SHRIMP U–Pb zircon dating are presented in Table 1. Zircons from gabbro samples RH02-3 and RH02-10 are mostly anhedral and 50 μm in diameter. All of the zircon grains are transparent and pale

Table 1
Dongfanghong gabbro SHRIMP U–Pb zircon data.

Sample No.	U (ppm)	Th (ppm)	Th/U	Pb (ppm)	$^{206}Pb_c$ (%)	$^{204}Pb/^{206}Pb$	$^{207}Pb^*/^{206}Pb^*$	±%	$^{207}Pb^*/^{235}U$	±%	$^{206}Pb^*/^{238}U$	±%	error	% Disc-ordance	$^{207}Pb/^{235}U$ Age (Ma)	1σ	$^{206}Pb/^{238}U$ Age (Ma)	1σ
RH02-3-01	228	198	0.87	11	0.66	0.0004	0.0470	6	0.28	7	0.0430	2	0.2	8	251	15	271	4
RH02-3-02	158	113	0.71	7	0.81	0.0004	0.0462	8	0.27	8	0.0429	2	0.2	9	247	17	271	5
RH02-3-03	80	39	0.49	3	3.41	0.0019	0.0318	31	0.19	31	0.0427	2	0.1	35	175	49	270	6
RH02-3-04	217	143	0.66	10	0.54	0.0003	0.0501	5	0.30	5	0.0430	2	0.3	2	265	12	272	4
RH02-3-05	127	106	0.84	6	0.67	0.0004	0.0499	7	0.30	7	0.0438	2	0.2	3	269	17	277	5
RH02-3-06	103	79	0.77	5	1.96	0.0011	0.0374	17	0.22	17	0.0426	2	0.1	25	203	31	269	5
RH02-3-07	98	77	0.79	4	1.24	0.0007	0.0477	13	0.28	13	0.0423	2	0.2	6	250	29	267	6
RH02-3-08	325	314	0.97	16	0.00	0.0000	0.0540	2	0.33	2	0.0438	2	0.6	4	288	6	277	4
RH02-3-09	56	24	0.44	2	0.00	0.0000	0.0563	5	0.34	6	0.0444	2	0.4	8	302	15	280	6
RH02-3-10	122	105	0.86	6	1.42	0.0008	0.0414	13	0.25	13	0.0435	2	0.1	18	226	26	275	5
RH02-3-11	80	63	0.79	4	1.42	0.0008	0.0491	13	0.30	13	0.0440	2	0.2	4	266	30	278	6
RH02-3-12	80	40	0.50	3	2.89	0.0016	0.0324	29	0.19	29	0.0434	2	0.1	34	181	48	274	6
RH02-3-13	372	311	0.84	18	0.00	0.0000	0.0544	2	0.33	2	0.0437	2	0.7	5	289	6	276	5
RH02-3-14	102	44	0.43	4	2.01	0.0011	0.0401	15	0.24	16	0.0439	2	0.1	20	222	31	277	5
RH02-3-15	224	153	0.68	10	0.14	0.0001	0.0524	3	0.32	4	0.0439	2	0.5	1	281	9	277	4
RH02-10-01	178	103	0.58	7	0.68	0.0004	0.0484	6	0.29	6	0.0428	1	0.2	5	256	13	270	4
RH02-10-02	487	505	1.04	18	0.20	0.0001	0.0498	3	0.29	3	0.0429	1	0.4	3	263	8	271	4
RH02-10-03	728	343	0.47	27	0.13	0.0001	0.0513	1	0.31	2	0.0439	1	0.6	0	276	5	277	3
RH02-10-04	735	778	1.06	28	0.14	0.0001	0.0512	1	0.31	2	0.0442	1	0.7	1	277	5	279	4
RH02-10-05	164	122	0.74	6	0.58	0.0003	0.0526	5	0.32	5	0.0438	2	0.3	2	281	13	276	5
RH02-10-06	62	43	0.70	2	0.35	0.0002	0.0557	9	0.33	9	0.0434	2	0.2	7	294	22	274	5
RH02-10-07	266	115	0.43	10	0.33	0.0002	0.0515	3	0.32	4	0.0448	2	0.5	0	282	9	283	5
RH02-10-08	118	46	0.39	4	5.67	0.0031	0.0334	28	0.20	28	0.0428	2	0.1	32	184	46	271	6
RH02-10-09	110	84	0.77	4	2.79	0.0015	0.0325	21	0.19	21	0.0427	2	0.1	34	178	34	270	4
RH02-10-10	105	84	0.80	4	3.34	0.0018	0.0349	32	0.20	32	0.0422	2	0.1	29	189	53	267	5
RH02-10-11	90	34	0.38	3	1.04	0.0006	0.0527	9	0.33	9	0.0449	2	0.2	2	288	22	284	5

Errors are 1-sigma; Pb_c indicates common ^{206}Pb. $^{*204}Pb$ corrected data.

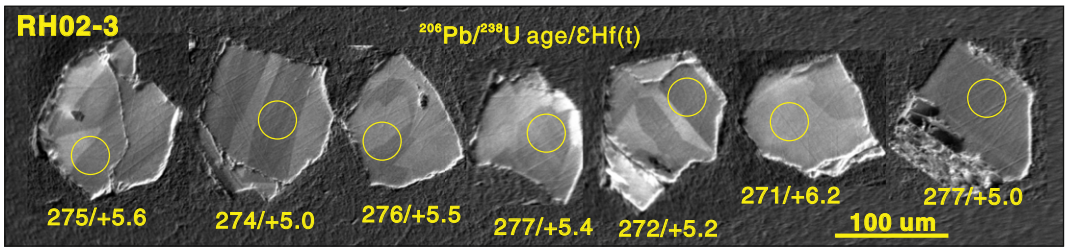

Fig. 4. CL images of representative zircons from gabbro sample RH02-3. Circles are the analysis sites and the ages are given in Ma.

yellow in color. Cathodoluminescence (CL) images (Fig. 4) show that most zircons have banded structure, indicating an origin in basic igneous rocks (Wan et al., 2005).

Fifteen zircon grains were analyzed from gabbro sample RH02-3. The measured U and Th concentrations vary from 56 to 372 ppm and from 24 to 314 ppm, respectively. The Th/U ratios range from 0.43 to 0.97. Five grains were excluded from the calculations because of large discordance (>10%). The remaining 10 analyses give a concordia age of 274 ± 4 Ma (MSWD = 1.4) and a $^{206}Pb/^{238}U$ weighted mean age of 275 ± 3 Ma (MSWD = 0.59) (Fig. 5a).

Eleven zircon grains were analyzed from gabbro sample RH02-10. The measured U and Th concentrations vary from 62 to 735 ppm and from 34 to 778 ppm, respectively. The Th/U ratios range from 0.38 to 1.06. Three grains were excluded from the calculations because of large discordance (>10%). The remaining eight analyses give a concordia age of 276 ± 3 Ma (MSWD = 1.9) and a $^{206}Pb/^{238}U$ weighted mean age of 276 ± 4 Ma (MSWD = 1.4) (Fig. 5b).

Taken together, the 18 concordant analyses define a concordia age of 275 ± 2 Ma (MSWD = 0.25) and a $^{206}Pb/^{238}U$ weighted average age of 275 ± 2 Ma (MSWD = 0.94), representing the crystallization age of the Dongfanghong gabbro.

5.2. Major element analyses

Major element analyses of the Dongfanghong gabbro samples RH02-1 to RH02-13 are presented in Table 2. After volatile-free correction, the 11 samples have SiO_2 contents of 50.2 to 52.7 wt.%, Na_2O of 2.0 to 3.2 wt.% and K_2O of 0.3 to 0.4 wt.% (Fig. 6a, b). They form two distinct groups based on differences in SiO_2 content. In the TAS diagram, the samples plot in the gabbro field, and belong to the sub-alkaline series (Fig. 6c). In the ΣFeO/MgO vs. SiO_2 diagram, they plot along the boundary between the calc-alkaline and tholeiite series (Fig. 6d). The MgO contents of 4.6–6.2 wt.% and Mg# values of 53 to 64 suggest that the parental magma experienced moderate amounts of fractionation (Fig. 6e, f). The gabbro is also characterized by high Al_2O_3 (19.5 to 22.3 wt.%) and high CaO (9.6 to 13.5 wt.%) (Fig. 6g, h), indicating a possible high-alumina parental melt with plagioclase accumulation.

5.3. Trace and rare earth element analyses

Trace and rare earth element analyses are presented in Table 2. The gabbro samples have ∑REE contents in the range of 21 to 29 ppm, with relatively high LREE/HREE ratios [$(La/Yb)_N$ of 3.2–4.0] and positive Eu anomalies (Eu/Eu^* = 1.47–2.37) (Fig. 7a). They show positive Ba, K, Pb, and Sr anomalies and depletion in high field strength elements (HFSE) Nb, Ta, P, Zr, and Hf (Fig. 7b). The enrichment in Sr and Eu support plagioclase accumulation as identified by the major element data. The negative Nb/Ta anomalies and enrichment of LILE suggest that the source was likely affected by subduction and/or the input of crustal material.

5.4. Sr–Nd–Pb–Hf isotopes

Sr–Nd–Pb isotopic data are listed in Table 3 and zircon Hf isotopic data are presented in Table 4.

The initial Sr–Nd–Pb-Hf isotopic compositions were calculated at 275 Ma. The Dongfanghong gabbro shows signatures of enriched mantle II (EM2), with initial $^{87}Sr/^{86}Sr$ ratios of 0.706379 to 0.706564, $\varepsilon_{Nd}(t)$ values from −0.77 to −0.39 (Fig. 8a), zircon $\varepsilon_{Hf}(t)$ values of +4.55 to +7.73 (Fig. 8b) with an average value of 5.8 ± 0.3 (MSWD = 4.7), $^{208}Pb/^{204}Pb_{(i)}$ values from 37.97 to 38.11, $^{207}Pb/^{204}Pb_{(i)}$ values from 15.56 to 15.57, and $^{206}Pb/^{204}Pb_{(i)}$ values from 18.12 to 18.32 (Fig. 8c, d).

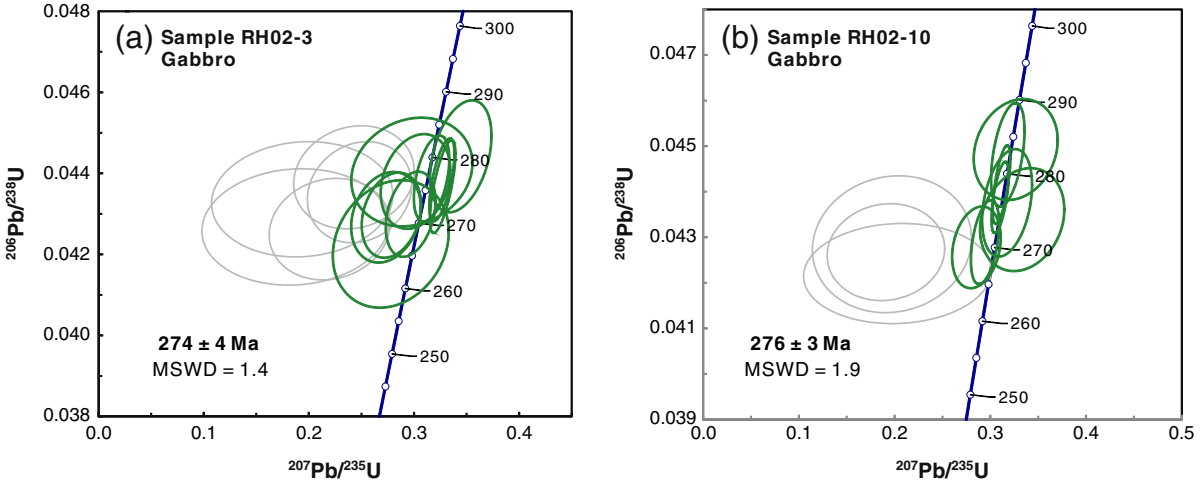

Fig. 5. SHRIMP zircon concordia diagrams for gabbro samples (a) RH02-3 and (b) RH02-10.

Table 2
Major and trace element data for the Dongfanghong gabbro.

Samples	RH02-1	RH02-2	RH02-3	RH02-4	RH02-5	RH02-8	RH02-9	RH02-10	RH02-11	RH02-12	RH02-13
SiO_2	50.45	50.83	50.64	50.24	50.36	47.99	48.47	48.78	51.46	49.48	49.56
TiO_2	0.54	0.52	0.56	0.48	0.46	0.51	0.60	0.50	0.59	0.79	0.62
Al_2O_3	19.23	19.49	19.25	18.90	18.72	21.29	20.51	19.99	20.11	19.19	18.98
Fe_2O_3	7.23	7.15	7.45	7.30	7.24	5.63	6.62	6.93	7.20	7.97	8.11
MnO	0.12	0.11	0.11	0.11	0.13	0.09	0.09	0.10	0.12	0.12	0.12
MgO	5.02	4.83	5.22	5.08	5.25	4.76	5.55	6.22	4.95	4.61	5.22
CaO	9.80	9.91	9.39	9.97	10.57	12.92	12.05	11.77	10.07	9.43	9.16
Na_2O	3.08	3.11	3.07	2.94	2.75	2.14	2.06	1.96	2.91	2.84	2.93
K_2O	0.42	0.39	0.40	0.40	0.34	0.25	0.27	0.27	0.25	0.35	0.29
P_2O_5	0.05	0.05	0.06	0.03	0.05	0.03	0.04	0.02	0.04	0.04	0.03
LOI	3.75	3.31	3.58	4.20	3.82	4.12	3.47	3.10	1.94	4.85	4.70
Total	99.69	99.70	99.74	99.65	99.70	99.73	99.72	99.65	99.63	99.68	99.72
Sc	25.4	23.4	25.4	26.9	31.2	27.5	31.7	29.1	28.1	25.8	27.6
Ti	3243	3078	3515	2828	2691	3089	3604	3125	3568	4898	3868
V	190	188	201	188	190	230	234	217	184	201	192
Cr	44	50	46	59	77	85	94	81	60	63	24
Mn	879	819	857	831	962	648	639	801	943	871	964
Co	30	41	27	26	30	26	29	29	32	29	30
Ni	10	15	10	11	11	20	40	20	19	32	13
Cu	8	17	8	7	7	12	11	7	10	12	10
Zn	61	62	64	61	61	51	55	58	65	71	71
Ga	18.3	18.6	18.2	17.9	18.0	18.3	17.1	17.5	19.5	19.3	19.2
Ge	1.9	1.9	1.9	1.8	1.9	1.4	1.7	1.8	1.9	1.9	1.9
Rb	8.8	7.3	9.2	8.7	7.3	3.8	4.2	6.2	3.4	7.6	5.5
Sr	499	483	498	491	477	502	466	479	466	475	476
Y	8.1	6.7	7.1	7.0	7.8	7.0	9.0	6.5	6.5	6.2	6.2
Zr	20.4	19.1	17.5	17.7	16.4	15.3	16.8	13.5	15.2	19.9	13.8
Nb	0.83	0.74	0.81	0.57	0.51	0.70	0.86	0.63	0.61	0.96	0.66
Cs	1.80	1.50	1.94	1.81	1.62	1.09	1.15	1.58	0.70	1.16	1.16
Ba	164	146	161	153	125	227	124	126	116	125	114
La	3.84	3.77	3.78	3.36	3.67	3.91	4.05	3.55	3.45	3.58	3.23
Ce	8.85	8.73	8.42	7.43	8.23	8.60	9.46	7.55	7.57	7.66	6.96
Pr	1.18	1.07	1.09	0.97	1.07	1.10	1.29	0.98	0.96	0.97	0.89
Nd	5.16	4.52	4.63	4.18	4.71	4.63	5.67	4.09	4.12	4.03	3.76
Sm	1.37	1.15	1.18	1.14	1.26	1.20	1.54	1.08	1.06	1.01	0.98
Eu	0.84	0.82	0.79	0.78	0.79	0.71	0.77	0.65	0.84	0.81	0.80
Gd	1.47	1.20	1.31	1.22	1.39	1.27	1.65	1.18	1.14	1.08	1.08
Tb	0.25	0.21	0.22	0.21	0.25	0.22	0.29	0.20	0.20	0.18	0.19
Dy	1.57	1.29	1.38	1.35	1.55	1.35	1.76	1.24	1.26	1.17	1.18
Ho	0.34	0.28	0.29	0.29	0.32	0.28	0.37	0.26	0.27	0.26	0.26
Er	0.90	0.75	0.80	0.79	0.88	0.77	0.98	0.73	0.75	0.72	0.71
Tm	0.13	0.11	0.12	0.12	0.13	0.11	0.14	0.11	0.11	0.11	0.11
Yb	0.82	0.72	0.74	0.76	0.83	0.69	0.87	0.68	0.73	0.71	0.71
Lu	0.13	0.11	0.12	0.12	0.13	0.11	0.13	0.10	0.12	0.11	0.11
Hf	0.68	0.59	0.57	0.55	0.55	0.52	0.62	0.47	0.48	0.58	0.45
Ta	0.07	0.07	0.06	0.05	0.05	0.06	0.07	0.05	0.05	0.07	0.05
Pb	1.99	3.20	3.14	2.76	2.71	3.61	3.16	3.28	2.68	3.18	3.08
Th	0.48	0.48	0.44	0.39	0.45	0.32	0.28	0.27	0.34	0.42	0.33
U	0.11	0.12	0.11	0.09	0.11	0.08	0.07	0.06	0.08	0.11	0.08

6. Discussion

6.1. Mantle source and tectonic discrimination of the Dongfanghong gabbro

The above petrological and geochemical results suggest that the parental magma of the Dongfanghong gabbro was derived from a water-saturated enriched mantle source that was most likely affected by subduction. The water/fluid-enriched condition is recognized by the presence of hornblende, enrichment in Al_2O_3, Eu and Sr, and also the depletion of HFSE. The low Ce/Pb (2.3–4.5) and Nb/U (4.6–12.9) ratios and Sr–Nd–Pb–Hf isotope signatures also suggest an enriched mantle source. The negative $\varepsilon_{Nd}(t)$ values suggest that the mantle source was enriched by addition of continental materials and/or recycling of old oceanic crust.

Tectonic discrimination diagrams suggest that the Dongfanghong gabbro was formed in an island arc. In the Th–Hf–Ta and La–Y–Nd discrimination diagrams (Fig. 9a, b), the Dongfanghong gabbro plots in the volcanic arc fields. In the K_2O–TiO_2–P_2O_5 discrimination diagram (Fig. 9c), it plots in the oceanic field. In the MnO–TiO_2–P_2O_5 discrimination diagram (Fig. 9d) which was designed for distinguishing the tectonic setting of oceanic basalts, it plots in the island arc tholeiite (IAT) field. In the Th/Yb vs. Nb/Yb and La/Yb vs. Th/Yb diagrams (Fig. 9e, f), the gabbro also plots in the field of intra-oceanic island arcs. In the V vs. Ti diagram (Fig. 9g), it also plots in the island arc tholeiite field. Combined with the relatively low K, it is concluded that the Dongfanghong gabbro most likely formed in an immature island arc.

6.2. Early Permian magmatic and sedimentary evolution of the eastern margin of the Jiamusi Block

The eastern margin of the Jiamusi Block also has Early Permian igneous rocks, including the Liulian Pluton in the northeast, the Erlongshan Formation in the east, and the Tiexi Pluton in the southeast (Fig. 2a). The Liulian hornblende gabbro has a zircon U–Pb age of 278 ± 2 Ma (Yu et al., 2013b), whereas the Erlongshan Formation andesite has a zircon U–Pb age of 293 ± 2 Ma (Meng et al., 2008) and the Tiexi diorite records a zircon U–Pb age of 296 ± 2 Ma (Yang et al., 2015). These Early Permian igneous rocks are mostly intermediate and characterized by high Na_2O (Fig. 6a), low K_2O (Fig. 6b), high Al_2O_3 (Fig. 6g), and are rich in LREE and LILE, but depleted in HFSE (Fig. 7a, b), with either no or weakly

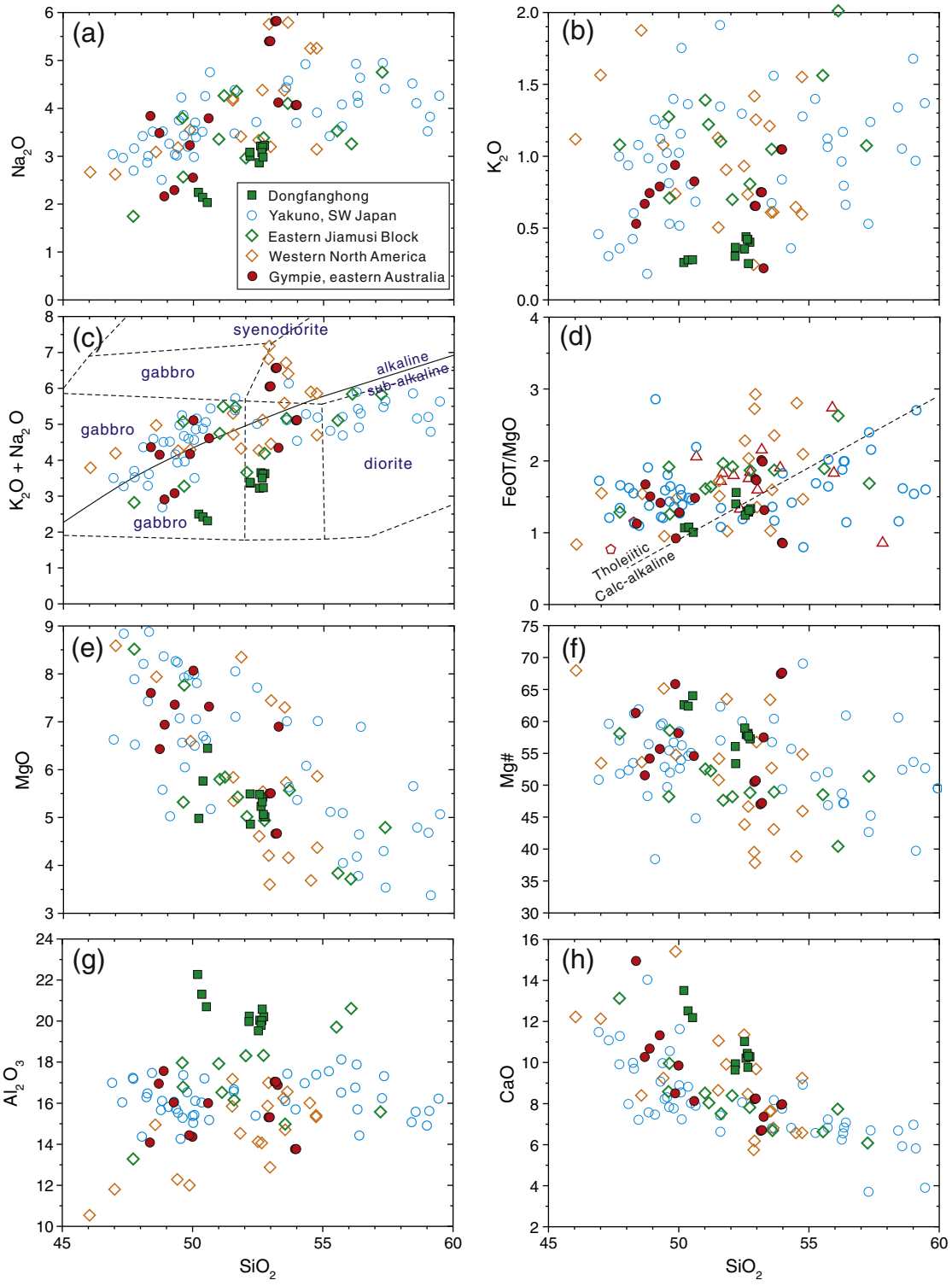

Fig. 6. Plots of major elements for the Dongfanghong gabbro samples (a) Na_2O vs. SiO_2; (b) K_2O vs. SiO_2; (c) TAS; (d) FeO^T/MgO vs. SiO_2; (e) MgO vs. SiO_2; (f) Mg# vs. SiO_2; (g) Al_2O_3 vs. SiO_2; (h) CaO vs. SiO_2. The data for the other basic–intermediate rocks are from Yakuno, SW Japan (Suda and Hayasaka, 2009), eastern Jiamusi Block (Meng et al., 2008; Yang et al., 2015; Yu et al., 2013b), western North American Craton (Blein et al., 2001) and Gympie, eastern Australia (Sivell and McCulloch, 2001; Sivell and Waterhouse, 1988).

positive Eu anomalies. They are thus different from the Permian intraplate high-K bimodal igneous rocks in the west of the Jiamusi Block and in the eastern CAOB (Meng et al., 2011). These rocks plot in the area of continental arcs in tectonic discrimination diagrams (Fig. 9c, e, f), indicating an immature continental arc setting (Condie and Crow, 1990; Pearce, 2014; Pearce et al., 1975).

The sedimentary sequences in the Jiamusi Block (Fig. 10) also support an active continental margin in the Permian. The eastern margin of the Jiamusi Block has Late Silurian quartz-rich sandstone, with basal quartz conglomerate overlying the basement composed of Pan-African Mashan Complex khondalitic rocks, granites and amphibolites. In the Devonian, fossiliferous reef limestone was deposited (Li, 2008). In the

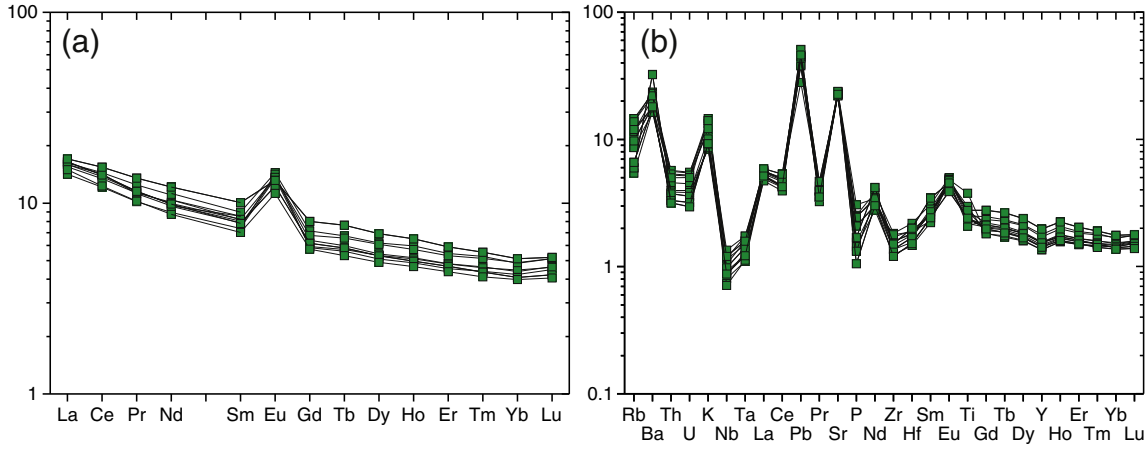

Fig. 7. (a) Chondrite normalized REE diagram and (b) primitive mantle normalized spider diagram for the gabbro samples (chondrite and primitive mantle normalization values after Sun and McDonough, 1989).

Carboniferous, limestone was continuously deposited, but was interleaved with coarse sandstone. These coastal shallow marine facies sedimentary rocks contain no igneous record, indicating a passive margin to the Jiamusi Block. Based on detrital zircon results (Dong, 2013), non-marine sedimentary rocks (with coal deposits) occurred after ~315 Ma. The change from shallow-marine to non-marine facies likely suggests a tectonic switch from passive margin to active margin. The Early Permian andesites (Meng et al., 2008) define the change to an active continental margin.

Therefore, the magmatic and sedimentary evidence both suggest that the initiation of an active continental margin along the eastern Jiamusi Block occurred in the earliest Early Permian.

6.3. Early Permian circum-Paleo-Pacific arc magmatism in SW Japan, western North America and eastern Australia

The Permian Dongfanghong gabbro and basic-intermediate igneous rocks in the Jiamusi Block were formed in an arc setting. Nevertheless it needs to be clarified whether this arc is related to paleo-Pacific subduction or to other subduction systems, such as the Paleo-Tethys or Paleo-Asian oceans.

Firstly, the location in the Wandashan Orogen suggests that the Dongfanghong gabbro is likely related to Paleo-Pacific subduction (Figs. 1 and 2) (see Wilde and Zhou, in press). Fig. 11a shows the Permian global plate reconstruction map from Xiao et al. (2015). A proposed modification is made in Fig. 11b, which shows the possible locations of the Jiamusi Block and the Dongfanghong arc, suggesting that Paleo-Pacific Ocean subduction was towards NE China from the east. The nomenclature 'Solonker Ocean', 'Panthalassa' and 'Amuria' in Xiao et al. (2015) are equivalent to 'Paleo-Asian Ocean', 'Paleo-Pacific Ocean' and 'Eastern CAOB', respectively.

Secondly, the timing does not support an origin from Paleo-Asian Ocean subduction. The initiation of an active continental margin along the southern CAOB (Paleo-Asian Ocean subduction) was much earlier, possibly in the Devonian (Li et al., 2010, 2014a; Zhao et al., 2013), whereas an active margin along the eastern Jiamusi Block did

Table 3
Whole rock Sr–Nd–Pb isotopic results for the Dongfanghong gabbro.

Sample	RH02-1	RH02-2	RH02-8	RH02-10	RH02-11	RH02-12	RH02-13
Age (Ma)	275	275	275	275	275	275	275
Rb (ppm)	8.82	7.29	3.79	6.19	3.44	7.58	5.45
Sr (ppm)	499.0	482.6	501.7	478.8	466.2	474.5	475.7
Rb/Sr	0.0177	0.0151	0.0076	0.0129	0.0074	0.0160	0.0115
$^{87}Rb/^{86}Sr$	0.0511	0.0437	0.0219	0.0374	0.0214	0.0462	0.0331
$^{87}Sr/^{86}Sr$	0.706695	0.706629	0.706649	0.706688	0.706462	0.706610	0.706533
2σ	8	8	6	6	7	8	7
$(^{87}Sr/^{86}Sr)_i$	0.706496	0.706459	0.706564	0.706542	0.706379	0.70643	0.706404
Sm (ppm)	1.37	1.15	1.20	1.08	1.06	1.01	0.98
Nd (ppm)	5.16	4.52	4.63	4.09	4.12	4.03	3.76
$^{147}Sm/^{144}Nd$	0.1607	0.1535	0.1567	0.1592	0.1550	0.1521	0.1578
$^{143}Nd/^{144}Nd$	0.512538	0.512528	0.512527	0.512551	0.512542	0.512527	0.512537
2σ	4	3	4	5	5	4	4
εNd(t)	−0.69	−0.64	−0.77	−0.39	−0.41	−0.61	−0.61
2σ	0.04	0.03	0.04	0.05	0.05	0.04	0.04
U (ppm)	0.11	0.12	0.08	0.06	0.08	0.11	0.08
Th (ppm)	0.48	0.48	0.32	0.27	0.34	0.42	0.33
Pb (ppm)	1.99	3.20	3.61	3.28	2.68	3.18	3.08
$(^{208}Pb/^{204}Pb)_m$	38.181	38.242	38.114	38.080	38.169	38.158	38.135
2σ	0.003	0.003	0.003	0.003	0.004	0.003	0.004
$(^{207}Pb/^{204}Pb)_m$	15.565	15.579	15.567	15.558	15.574	15.564	15.561
2σ	0.001	0.001	0.001	0.001	0.002	0.001	0.002
$(^{206}Pb/^{204}Pb)_m$	18.281	18.420	18.310	18.305	18.369	18.356	18.311
2σ	0.001	0.002	0.001	0.001	0.002	0.002	0.002
$(^{208}Pb/^{204}Pb)_t$	37.967	38.106	38.035	38.007	38.056	38.038	38.040
$(^{207}Pb/^{204}Pb)_t$	15.556	15.574	15.564	15.555	15.57	15.56	15.557
$(^{206}Pb/^{204}Pb)_t$	18.124	18.320	18.253	18.253	18.284	18.265	18.240

Table 4
In situ zircon Hf isotopic data for the Dongfanghong gabbro.

Spot#	Age (Ma)	$^{176}Yb/^{177}Hf$	±2σ	$^{176}Lu/^{177}Hf$	±2σ	$^{176}Hf/^{177}Hf$	±2σ	εHf(t)	±2σ
RH02-3-01	275	0.05226	0.00051	0.001503	0.000010	0.282786	0.000010	5.88	0.28
RH02-3-02	275	0.02575	0.00041	0.000728	0.000009	0.282780	0.000010	5.81	0.74
RH02-3-03	275	0.05448	0.00066	0.001585	0.000014	0.282770	0.000012	5.30	0.81
RH02-3-04	275	0.02384	0.00007	0.000692	0.000003	0.282752	0.000010	4.83	0.74
RH02-3-05	275	0.05452	0.00097	0.001522	0.000027	0.282742	0.000009	4.32	0.71
RH02-3-06	275	0.06320	0.00067	0.001811	0.000021	0.282739	0.000010	4.16	0.75
RH02-3-07	275	0.02574	0.00005	0.000779	0.000002	0.282770	0.000009	5.45	0.71
RH02-3-08	275	0.05501	0.00020	0.001611	0.000008	0.282807	0.000009	6.60	0.71
RH02-3-09	275	0.02680	0.00044	0.000706	0.000010	0.282738	0.000013	4.33	0.85
RH02-3-10	275	0.02812	0.00018	0.000804	0.000004	0.282764	0.000009	5.23	0.71
RH02-3-11	275	0.03268	0.00010	0.000982	0.000002	0.282804	0.000010	6.61	0.74
RH02-3-12	275	0.02649	0.00028	0.000870	0.000012	0.282748	0.000010	4.65	0.74
RH02-3-13	275	0.02298	0.00022	0.000683	0.000007	0.282759	0.000009	5.08	0.71
RH02-3-14	275	0.03821	0.00035	0.001165	0.000011	0.282757	0.000009	4.92	0.71
RH02-3-15	275	0.02100	0.00014	0.000636	0.000005	0.282744	0.000010	4.55	0.74
RH02-10-01	275	0.02138	0.00009	0.000677	0.000003	0.282823	0.000011	7.34	0.77
RH02-10-02	275	0.04669	0.00028	0.001354	0.000007	0.282788	0.000017	5.98	0.99
RH02-10-03	275	0.03047	0.00046	0.000924	0.000013	0.282776	0.000009	5.63	0.71
RH02-10-04	275	0.06203	0.00186	0.001820	0.000044	0.282770	0.000016	5.26	0.96
RH02-10-05	275	0.01930	0.00009	0.000596	0.000002	0.282810	0.000011	6.90	0.78
RH02-10-06	275	0.03778	0.00007	0.001156	0.000006	0.282776	0.000013	5.59	0.85
RH02-10-07	275	0.03682	0.00012	0.001156	0.000009	0.282811	0.000011	6.83	0.78
RH02-10-08	275	0.02413	0.00012	0.000692	0.000002	0.282796	0.000011	6.38	0.78
RH02-10-09	275	0.05742	0.00019	0.001747	0.000001	0.282763	0.000011	5.02	0.78
RH02-10-10	275	0.02861	0.00034	0.000857	0.000013	0.282778	0.000016	5.72	0.96
RH02-10-11	275	0.02996	0.00009	0.000877	0.000001	0.282778	0.000010	5.71	0.74

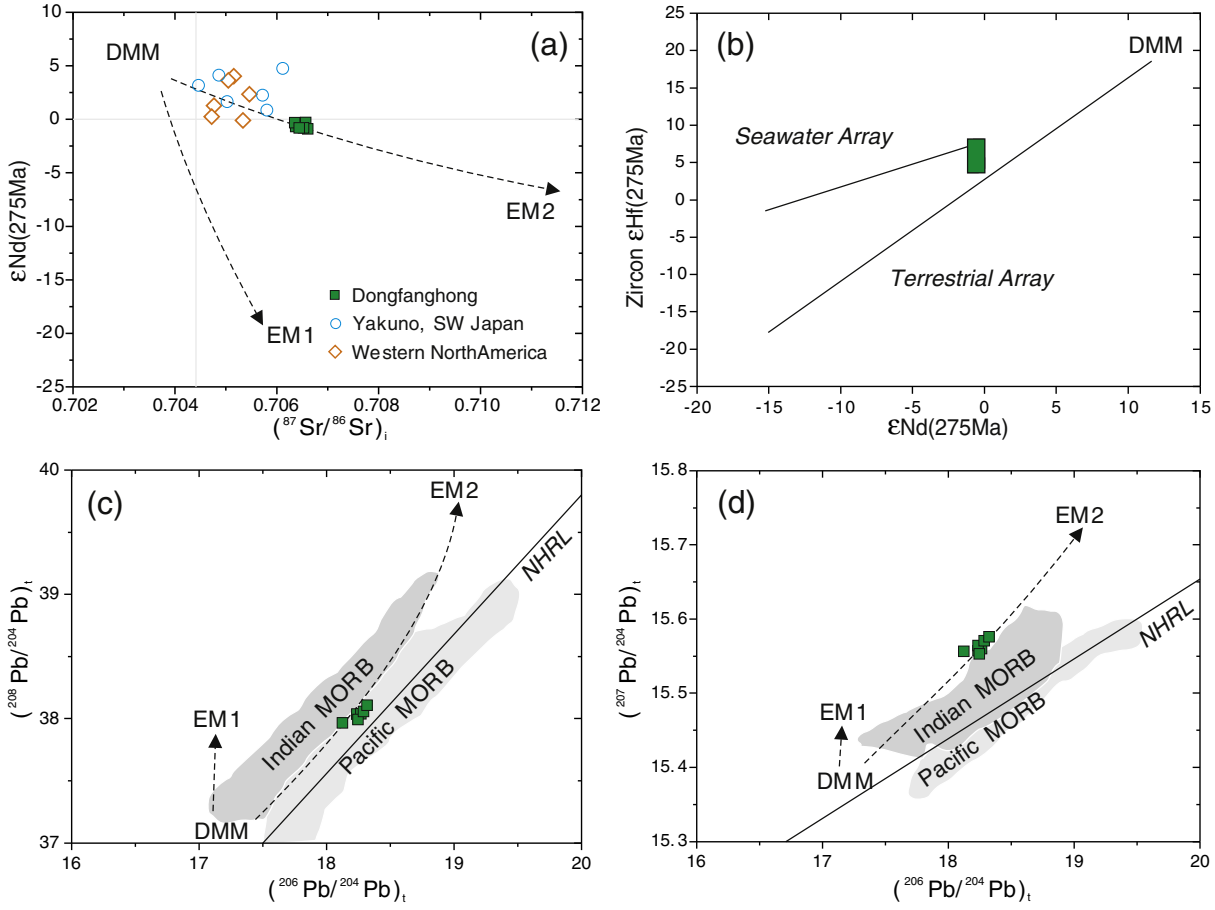

Fig. 8. (a) εNd(t) vs. initial $^{87}Sr/^{86}Sr$ ratio; (b) zircon εHf(t) vs. εNd(t) (after Vervoort et al., 2011); (c) $^{208}Pb/^{204}Pb_{(i)}$ vs. $^{206}Pb/^{204}Pb_{(i)}$; (d) $^{207}Pb/^{204}Pb_{(i)}$ vs. $^{206}Pb/^{204}Pb_{(i)}$ showing an enriched mantle source for the Dongfanghong gabbro. Data for Permian igneous rocks of SW Japan (Sano, 1992) and Western USA (Blein et al., 2001) are also plotted. DMM: depleted MORB mantle; EM1: Enriched Mantle I; EM2: Enriched Mantle II; NHRL: Northern Hemisphere Reference Line (after Hart, 1984).

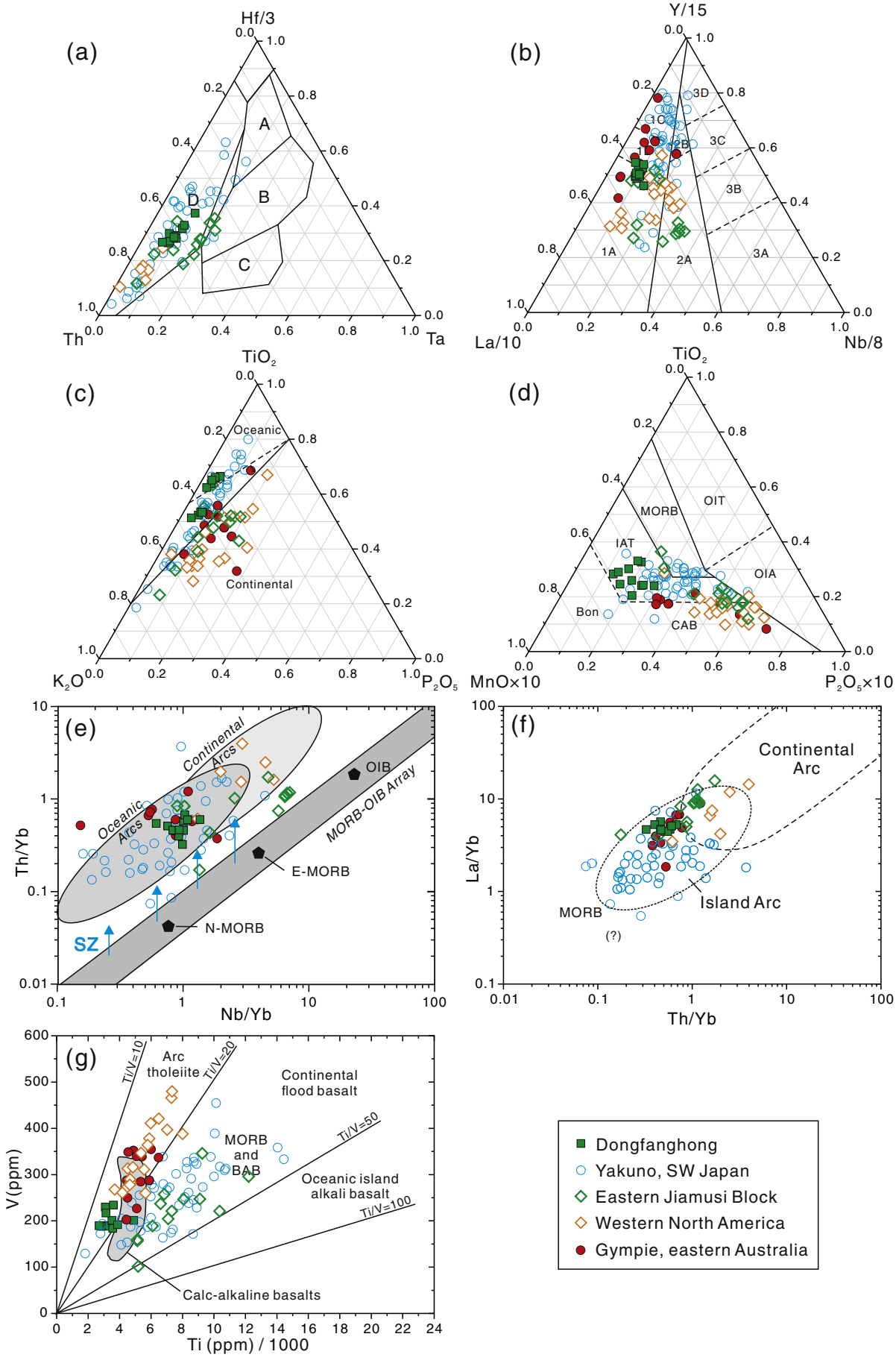
(a)
Hf/3
Th
Ta
A
B
C
D
(b)
Y/15
La/10
Nb/8
1A
2A
3A
1B
2B
3B
1C
2C
3C
3D
(c)
TiO2
K2O
P2O5
Oceanic
Continental
(d)
TiO2
MnO×10
P2O5×10
MORB
OIT
IAT
OIA
CAB
Bon
(e)
Th/Yb
Nb/Yb
Continental Arcs
Oceanic Arcs
OIB
MORB-OIB Array
E-MORB
N-MORB
SZ
(f)
La/Yb
Th/Yb
Continental Arc
Island Arc
MORB
(?)
(g)
V (ppm)
Ti (ppm) / 1000
Ti/V=10
Ti/V=20
Ti/V=50
Ti/V=100
Arc tholeiite
Continental flood basalt
MORB and BAB
Oceanic island alkali basalt
Calc-alkaline basalts
Dongfanghong
Yakuno, SW Japan
Eastern Jiamusi Block
Western North America
Gympie, eastern Australia

not occur until the earliest Permian (Section 6.2), thus such subduction initiation cannot be caused by Paleo-Asian Ocean subduction.

Thirdly, Permian arc rocks along the circum Paleo-Pacific Ocean margin, as shown in the modified Permian global plate reconstruction map (Fig. 11b), are also reported in the Yakuno Ophiolite, SW Japan (Sano, 1992); from Nevada, at the western margin of the North American Craton (Blein et al., 1994) and at Gympie in eastern Australia (Sivell and Waterhouse, 1988).

The spatial and time configurations thus likely link the Dongfanghong gabbro with the westward subduction of the Paleo-Pacific Ocean. We therefore compare the geochemical signatures of these contemporaneous arc magmatic rocks.

6.3.1. Yakuno Ophiolite, SW Japan

In southwest Japan, Permian island arc magmatism is recorded on Honshu Island, represented by the "Yakuno Ophiolite" (Ishiwatari, 1985; Ishiwatari and Tsujimori, 2003) (Fig. 11). The Yakuno Ophiolite records an intra-oceanic island-arc–back-arc basin system along the East Asian continent (Suda et al., 2014). It consists of three different segments, which, from bottom to top, include an unusually thick oceanic crust (lower unit), island arc crust (middle unit) and oceanic back-arc basin (upper unit) (Ichiyama and Ishiwatari, 2004). The middle unit of the Yakuno Ophiolite is comparable to the Dongfanghong gabbro. The metabasalts in the middle unit have Rb–Sr whole rock radiometric ages of ~285 Ma (Sano, 1992). Zircons from plagiogranites in the middle unit have yielded similar U–Pb ages of 285 ± 2 Ma and 282 ± 2 Ma (Herzig et al., 1997). Recent SHRIMP U–Pb zircon dating shows that the amphibolite and metagabbro of the middle–upper unit of the Yakuno Ophiolite have ages of 293 ± 10 Ma and 288 ± 13 Ma (Suda et al., 2014). The basic–intermediate rocks (mainly hornblende gabbro) in the middle unit of the Yakuno Ophiolite are mostly characterized by high Na_2O (Fig. 6a), low to medium K_2O (Fig. 6b), and high Al_2O_3 contents (Fig. 6g), and are rich in LREE and LILE and low in HFSE (Fig. 7a, b). In the Th–Hf–Ta and La–Y–Nd discrimination diagrams (Fig. 9a, b), they mainly plot in the volcanic arc field, together with the Dongfanghong gabbro. In the K_2O–TiO_2–P_2O_5 discrimination diagram, they plot mainly in the oceanic region or near the boundary between oceanic and continental regions (Fig. 9c). In the Th/Yb vs. Nb/Yb and La/Yb vs. Th/Yb diagrams (Fig. 9e, f), they again mostly plot in the area of intra-oceanic island arcs. Thus the basic–intermediate rocks in the middle unit of the Yakuno Ophiolite are comparable to the Dongfanghong gabbro from both geochronology and geochemistry, with the latter indicating an immature island arc tectonic setting.

6.3.2. Western margin of the North American Craton

The western margin of the North America also contains Permian igneous rocks, present in western Nevada and the northern Sierra Nevada, and represented by Lower Permian volcanic suites of the Black Dyke and Goodhue formations (Blein et al., 1994, 1996, 1999, 2001; Bourdier et al., 1991; Lapierre et al., 1994; Rouer et al., 1988). The Black Dyke Formation mainly consists of breccias, conglomerates and basaltic lavas, with fragments of pargasite-bearing gabbroic cumulates, that also occur as xenoliths in the lavas. Amphibole from the hornblende-bearing gabbroic cumulates records an $^{40}Ar/^{39}Ar$ age of 276 ± 2 Ma (Blein et al., 1999). The basic-intermediate rocks in the Black Dyke Formation are mostly characterized by high Na_2O (Fig. 6a), low K (Fig. 6b), and low Al_2O_3 contents (Fig. 6g), and are rich in LREE and LILE and low in HFSE

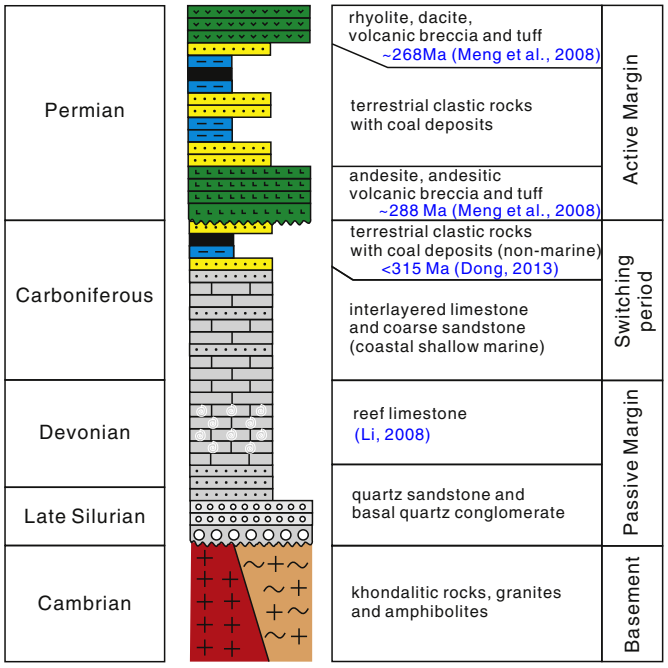

Fig. 10. Simplified stratigraphic column for the eastern margin of the Jiamusi Block (after HBGMR, 1981; Li and Li, 2007; Li, 2008; Dong, 2013).

(Fig. 7a, b). In tectonic discrimination diagrams, they plot in the same field as the Early Permian arc rocks of the eastern Jiamusi Block. In the Th–Hf–Ta and La–Y–Nd discrimination diagrams (Fig. 9a, b), the basic–intermediate rocks in the Black Dyke Formation plot in the volcanic arc field and in the K_2O–TiO_2–P_2O_5 discrimination diagram, they mainly plot in the continental region (Fig. 9c). In the Th/Yb vs. Nb/Yb and La/Yb vs. Th/Yb diagrams (Fig. 9e, f), they again plot in the area of continental arcs. Considering the above geochemical signatures, the basic–intermediate rocks in the Black Dyke Formation were most likely derived in a similar tectonic environment to the Early Permian arc rocks in the eastern Jiamusi Block (6.2), both in immature continental arc tectonic settings.

6.3.3. New England Orogen, eastern Australia

The New England Orogen in eastern Australia formed along a Paleozoic active continental margin (Aitchison and Flood, 1992; Harrington and Korsch, 1985; Phillips and Offler, 2011). The Gympie Group volcanics are recognized as remnants of an early Permian volcanic arc (Sivell and Waterhouse, 1988). A Permian intra-oceanic volcanic arc is also preserved in the Brook Street Terrane, New Zealand (Spandler et al., 2005). The Gympie Group was further constrained as part of an island arc (Sivell and Mcculloch, 2001) due to high Nd–isotope ratios [εNd (270 Ma) = +7.4 to +8.1] and geochemical features (e.g. high Zr/Nb, Sr/Nd and La/Nb) that reflect depleted asthenospheric mantle sources metasomatized by hydrous fluids from subducted lithosphere. The Gympie Group basalt plots together with the other Permian arc rocks in the major element diagrams (Fig. 6) and tectonic discrimination diagrams (Fig. 9), showing immature island arc signatures.

The more positive Nd isotope values of the Gympie arc rocks suggest that the recycling oceanic lithosphere towards eastern Australia in the

Fig. 9. Tectonic discrimination diagrams for Permian igneous rocks of the Paleo-Pacific domain. (a) Th–Hf–Ta (after Wood, 1980). The fields are: A, N-type MORB; B, E-type MORB and within-plate tholeiites; C, alkaline within-plate basalts; D, volcanic-arc basalts. (b) La/10–Y/15–Nd/8 (after Cabanis and Lecolle, 1989). Field 1, volcanic-arc basalt; field 2, continental basalt; and field 3, oceanic basalt. The subdivision of the fields are: 1A, calc-alkaline basalts; 1C, volcanic-arc tholeiites; 1B is the overlap between 1A and 1C; 2A, continental basalts; 2B, back-arc tholeiites; 3A, alkali basalts from intercontinental rift; 3B, 3C, E-type MORB (3B enriched, 3C weakly enriched); 3D, N-type MORB. (c) K_2O–TiO_2–P_2O_5 (after Pearce et al., 1975). (d) MnO–TiO_2–P_2O_5 (after Mullen, 1983). The fields are MORB—mid-ocean ridge basalt, OIT—oceanic island tholeiite, OIA—oceanic island alkali basalt, CAB—island-arc calc-alkaline basalt, IAT—island-arc tholeiite, Bon—boninite. (e) Th/Yb vs. Nb/Yb (after Pearce, 2014). (f) La/Yb vs. Th/Yb (after Condie and Crow, 1990). (g) V vs. Ti (after Shervais, 1982; Pearce, 2014). Data for the eastern Jiamusi Block from Meng et al. (2008), Yu et al. (2013b) and Yang et al. (2015); for SW Japan from Suda and Hayasaka (2009), for the Western USA from Blein et al. (2001), and for Gympie in eastern Australia from Sivell and Waterhouse (1988) and Sivell and McCulloch (2001).

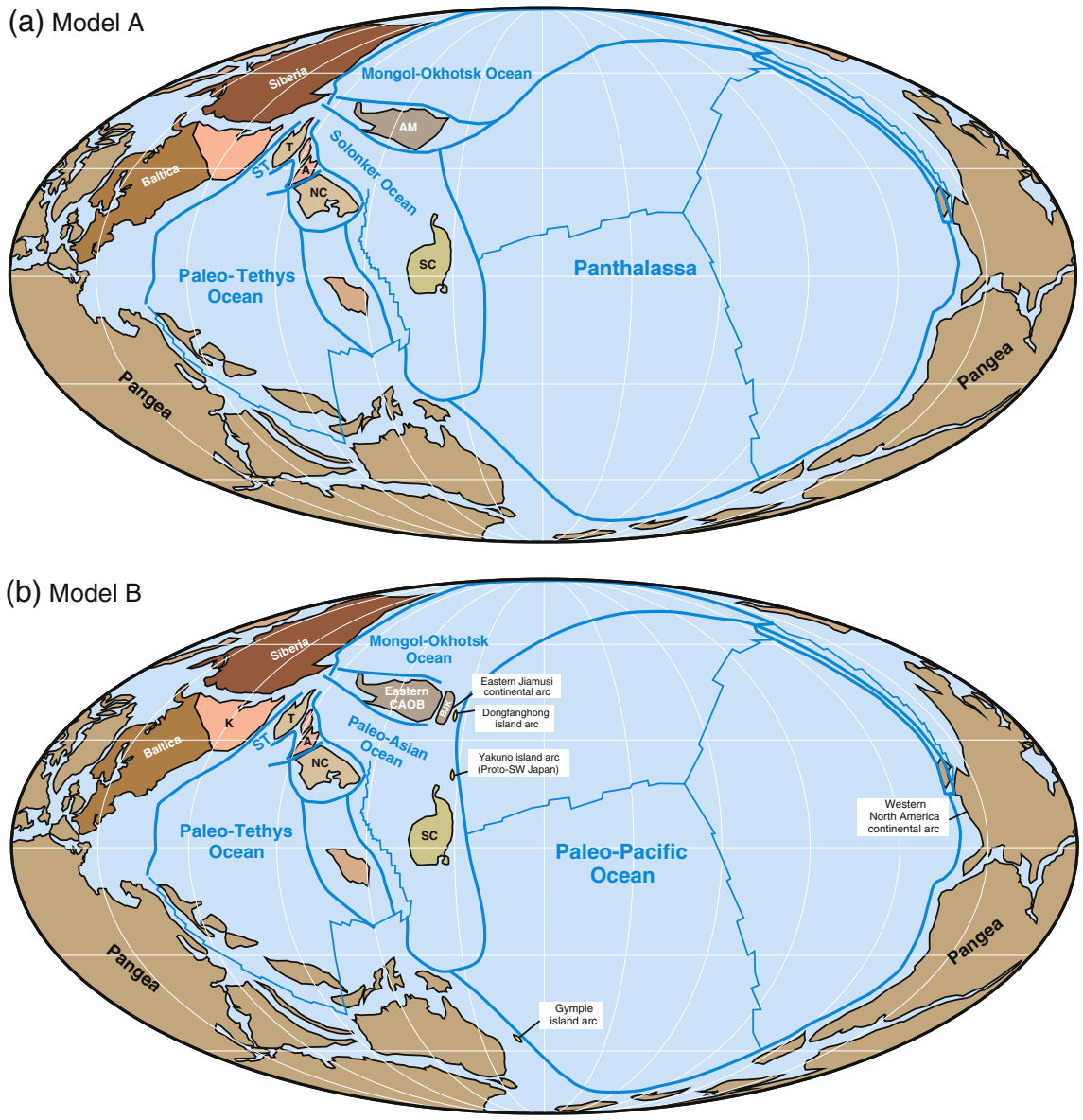

Fig. 11. (a) Permian global plate reconstruction map (from Xiao et al., 2015. The Central Meridian is 90° moved. The projected coordinate system is World_Mollweide, A: Alxa, AM: Amuria, K: Kazakhstan, NC: North China Craton, SC: South China Craton, ST: Southern Tianshan Ocean, T: Tarim Craton). (b) Modified Permian global plate reconstruction map showing the locations of the Paleo-Pacific Dongfanghong, Eastern Jiamusi, Yakuno, Western North America and Gympie areas (after Ueno, 2003; Lawver et al., 2009; Angiolini et al., 2015; Li et al., 2014b; Xiao et al., 2015).

Permian was younger than the one that subducted beneath NE China. This is consistent with the fact that an active continental margin occurred much earlier in eastern Australia represented by the Ordovician Macquarie Arc (Glen et al., 2011) under which old Paleo-Pacific lithosphere was already subducted.

6.4. Tectonic evolution model

The above discussion shows the geochemical similarities and differences of Permian arc rocks along the circum Paleo-Pacific margin. Thus we need to evaluate whether they formed under similar tectonic conditions.

For eastern Australia, when combined with data from the Carboniferous Connors–Auburn Arc and the exhumation history of eclogite and blueschist, the formation of the Gympie intra-oceanic arc is consistent with Permian arc retreat and slab roll-back (Phillips and Offler, 2011; Rosenbaum et al., 2012) (Fig. 12c, d).

We suggest that this model is also applicable for the tectonic evolution of NE China (Fig. 12a, b). The initiation of westward subduction of the Paleo-Pacific plate toward the Jiamusi Block possibly occurred in the earliest Early Permian, resulting in immature continental arc magmatism along the eastern margin of the Jiamusi Block at ~290 Ma. The intra-oceanic Dongfanghong island arc was developed off-shore to the east, with formation of the Dongfanghong gabbro at ~275 Ma, indicating a transition from a continental arc to an island arc, most likely related to slab roll-back. The collision between the Dongfanghong island arc and the Jiamusi Block probably occurred in the Early Mesozoic, forming the Yuejinshan Complex (Zhou et al., 2014), which is comparable to the Tablelands Complex in the New England Orogen.

Thus there are similarities between the Late Paleozoic to Early Mesozoic tectonic evolution of the eastern margin of Australia and the eastern margin of the Jiamusi Block. Both of them experienced a transition from continental arc to island arc formation in the Permian. Proto-SW Japan, as part of the western Paleo-Pacific, might also have experienced similar events, as recorded by the Yakuno Ophiolite. However, it

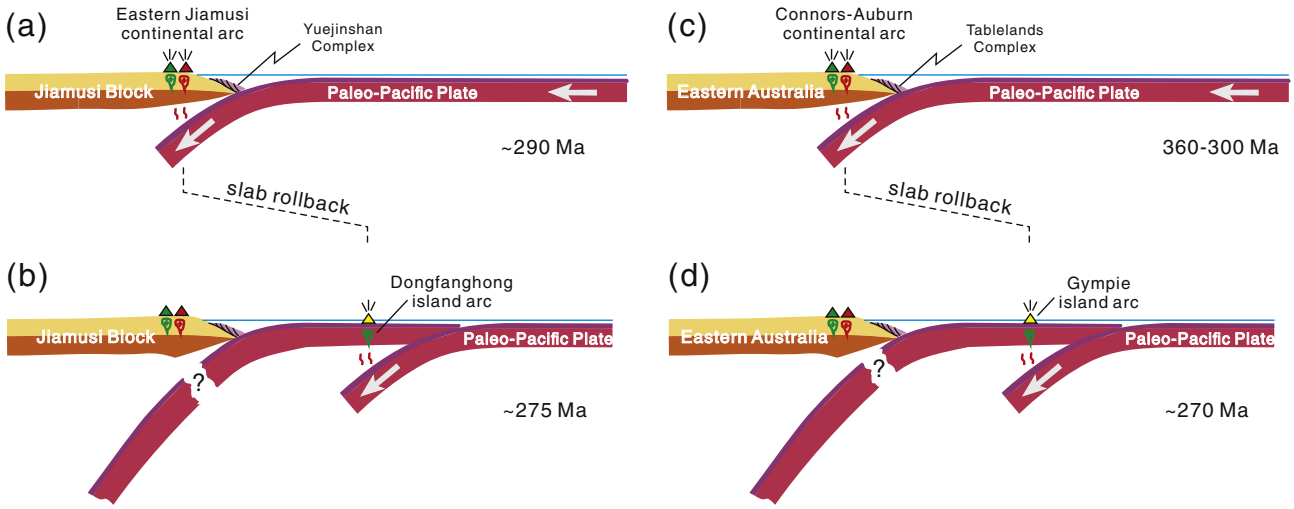

Fig. 12. Permian tectonic model for Paleo-Pacific subduction involving (a, b) the Jiamusi Block and the Dongfanghong island arc and (c, d) eastern Australia and the Gympie island arc. The tectonic model for eastern Australia is after Phillips and Offler (2011) and Li et al. (2014b).

remains controversial due to lack of evidence for a corresponded continental arc.

The above rollback model is based on the assumption that the gabbro is autochthonous. An alternative interpretation that the Dongfanghong gabbro was formed within the Paleo-Pacific Ocean by ocean-ocean subduction and was then incorporated into the accretion complex in the Mesozoic is also possible. However, when combining the record of magmatism and sedimentary evolution of NE China, arc magmatism in SW Japan, South China, Eastern Australia and North America, and also the history of Paleo-Asian and Paleo-Pacific oceans, we prefer the Paleo-Pacific subduction roll-back model to interpret the formation of the Dongfanghong gabbro.

7. Conclusions

SHRIMP U–Pb zircon dating and whole-rock geochemical and Sr–Nd–Pb isotopic analysis of the Dongfanghong gabbro allow us to determine its age and tectonic setting. When compared with the Early Permian igneous rocks along the eastern margin of the Jiamusi Block, western margin of the North American Craton, SW Japan and eastern Australia, we are able to draw the following conclusions:

(1) The SHRIMP U–Pb zircon age of the Dongfanghong gabbro is 275 ± 2 Ma.
(2) The geochemical and Sr–Nd–Pb and zircon Hf isotopic results suggest the Dongfanghong gabbro was derived from an EM2 mantle source.
(3) The Dongfanghong gabbro is a fragment of an immature island arc of the Paleo-Pacific Ocean.
(4) Paleo-Pacific subduction towards the Jiamusi Block occurred in the earliest Permian. Roll-back of the Paleo-Pacific plate also occurred in the Early Permian, prior to final amalgamation of the island arc with the East Asian continent in the Early Mesozoic.

Acknowledgements

We thank Kefeng Zhang, Taoyang Shao and Minna A for their help in the field. We appreciate the assistance of Adam Frew and Hao Gao during SHRIMP analysis at Curtin University and Le Zhang for zircon Hf analysis at the Guangzhou Institute of Geochemistry, Chinese Academy of Sciences. We appreciate the assistance of Ying Liu, Guangqian Hu and Jinlong Ma for major and trace element and Sr–Nd–Pb isotopic analyses at the Guangzhou Institute of Geochemistry, Chinese Academy of Sciences. We also appreciate discussions with Dr. John Wakabayashi. This work was supported by the China Postdoctoral Science Foundation (Grant No. 2014M560678), National Natural Science Foundation of China (Grant No. 91014007), National Program on Key Basic Research Project (973 Program, Grant No. 2011CB808906), and External Cooperation Program of Chinese Academy of Sciences (Grant No. 132744KYSB20130005). This is TIGeR publication number 636.

References

Aitchison, J.C., Flood, P.G., 1992. Early Permian transform margin development of the southern New-England Orogen, Eastern Australia (Eastern Gondwana). Tectonics 11, 1385–1391.
Angiolini, L., Zanchi, A., Zanchetta, S., Nicora, A., Vuolo, I., Berra, F., Henderson, C., Malaspina, N., Rettori, R., Vachard, D., Vezzoli, G., 2015. From rift to drift in South Pamir (Tajikistan): Permian evolution of a Cimmerian terrane. J Asian Earth Sci 102, 146–169.
Black, L.P., Kamo, S.L., Allen, C.M., Aleinikoff, J.N., Davis, D.W., Korsch, R.J., Foudoulis, C., 2003. TEMORA 1: a new zircon standard for Phanerozoic U–Pb geochronology. Chem. Geol. 200, 155–170.
Blein, O., Lapierre, H., Schweickert, R.A., Monie, P., Pecher, A., 1994. The Permian Black Dyke Formation (West-Central Nevada)—easternmost remnant of the Sierra-Nevada Paleozoic Arc. C. R. Acad. Sci. II 319, 201–208.
Blein, O., Lapierre, H., Schweicker, R.A., Monie, P., Maluski, H., Pecher, A., 1996. Remnants of the northern Sierra Nevada Paleozoic island arc in western Nevada. J. Geol. 104, 485–492.
Blein, O., Lapierre, H., Schweickert, R.A., Pecher, A., Monie, P., Maluski, H., Charvet, J., 1999. Age and depositional setting of the Permian Black Dyke Formation: implications for the paleogeography and structural evolution of western Nevada. Geodin. Acta 12, 321–340.
Blein, O., Lapierre, H., Schweickert, R.A., 2001. A Permian island-arc with a continental basement: the Black Dyke Formation (Nevada), North American Cordillera. Chem. Geol. 175, 543–566.
Bourdier, J.L., Rouer, O., Lapierre, H., 1991. The Mills peak volcanic and volcaniclastic sequence, an on-land fragment of a former seamount in the Paleozoic Island-Arc of Northern Sierra-Nevada, California. Bull. Soc. Geol. Fr. 162, 1049–1056.
Bouvier, A., Vervoort, J.D., Patchett, P.J., 2008. The Lu–Hf and Sm–Nd isotopic composition of CHUR: constraints from unequilibrated chondrites and implications for the bulk composition of terrestrial planets. Earth Planet. Sci. Lett. 273, 48–57.
Cabanis, B., Lecolle, M., 1989. The La/10-Y/15-Nb/8 diagram—a tool for discrimination volcanic series and evidencing continental-crust magmatic mixtures and or contamination. C. R. Acad. Sci. II 309, 2023–2029.
Cao, H.H., Xu, W.L., Pei, F.P., Guo, P.Y., Wang, F., 2012. Permian tectonic evolution of the eastern section of the northern margin of the North China Plate: Constraints from zircon U-Pb geochronology and geochemistry of the volcanic rocks. Acta Petrol Sin 28, 2733–2750.
Chen, C.H., Lee, C.Y., Shinjo, R.I., 2008. Was there Jurassic paleo-Pacific subduction in South China?: constraints from (40)Ar/(39)Ar dating, elemental and Sr–Nd–Pb isotopic geochemistry of the Mesozoic basalts. Lithos 106, 83–92.
Cheng, R.Y., Wu, F.Y., Ge, W.C., Sun, D.Y., Liu, X.M., Yang, J.H., 2006. Emplacement age of the Raohe Complex in eastern Heilongjiang Province and the tectonic evolution of the eastern part of Northeastern China. Acta Petrol. Sin. 22, 353–376.

Condie, K.C., Crow, C., 1990. Early Precambrian within-plate basalts from the Kaapvaal Craton in Southern-Africa—a case for crustally contaminated komatiites. J. Geol. 98, 100–107.
Dong, C., 2013. Tectonic evolution of the Jiamusi Massif: constraints from late Paleozoic sedimentary-volcanic rocks (Doctoral Thesis) Jilin University.
Donskaya, T.V., Gladkochub, D.P., Mazukabzov, A.M., Ivanov, A.V., 2013. Late Paleozoic–Mesozoic subduction-related magmatism at the southern margin of the Siberian continent and the 150 million-year history of the Mongol-Okhotsk Ocean. J. Asian Earth Sci. 62, 79–97.
Fan, W.M., Wang, Y.J., Zhang, A.M., Zhang, F.F., Zhang, Y.Z., 2010. Permian arc-back-arc basin development along the Ailaoshan tectonic zone: geochemical, isotopic and geochronological evidence from the Mojiang volcanic rocks, Southwest China. Lithos 119, 553–568.
Glen, R.A., Saeed, A., Quinn, C.D., Griffin, W.L., 2011. U–Pb and Hf isotope data from zircons in the Macquarie Arc, Lachlan Orogen: implications for arc evolution and Ordovician palaeogeography along part of the east Gondwana margin. Gondwana Res. 19, 670–685.
Grebennikov, A.V., Popov, V.K., 2014. Petrogeochemical aspects of the Late Cretaceous and Paleogene ignimbrite volcanism of East Sikhote-Alin. Russ. J. Pac. Geol. 8, 38–55.
Guo, F., Fan, W.M., Gao, X.F., Li, C.W., Miao, L.C., Zhao, L.A., Li, H.X., 2010. Sr–Nd–Pb isotope mapping of Mesozoic igneous rocks in NE China Constraints on tectonic framework and Phanerozoic crustal growth. Lithos 120, 563–578.
Harrington, H.J., Korsch, R.J., 1985. Tectonic model for the Devonian to Middle Permian of the New-England Orogen. Aust. J. Earth Sci. 32, 163–179.
Hart, S.R., 1984. A large-scale isotope anomaly in the Southern-Hemisphere mantle. Nature 309, 753–757.
HBGMR (Heilongjiang Bureau of Geology and Mineral Resources) (1981), 1:200 000 Regional Geological Survey Report of Baoqing (L-53-13) [in Chinese]. Geological Publishing House, Beijing, pp. 9–24
HBGMR (Heilongjiang Bureau of Geology and Mineral Resources) (1987), 1:200 000 Regional Geological Survey Report of Zhenbaodao (L-53-14) [in Chinese]. Geological Publishing House, Beijing, pp. 14–51.
Hennig, D., Lehmann, B., Frei, D., Belyatsky, B., Zhao, X.F., Cabral, A.R., Zeng, P.S., Zhou, M.F., Schmidt, K., 2009. Early Permian seafloor to continental arc magmatism in the eastern Paleo-Tethys: U–Pb age and Nd-Sr isotope data from the southern Lancangjiang zone, Yunnan, China. Lithos 113, 408–422.
Herzig, C.T., Kimbrough, D.L., Hayasaka, Y., 1997. Early Permian zircon uranium-lead ages for plagiogranites in the Yakuno Ophiolite, Asago district, southwest Japan. Island Arc 6, 396–403.
Ichiyama, Y., Ishiwatari, A., 2004. Petrochemical evidence for off-ridge magmatism in a back-arc setting from the Yakuno Ophiolite, Japan. Island Arc 13 (1), 157–177.
Ishiwatari, A., 1985. Igneous petrogenesis of the Yakuno Ophiolite (Japan) in the context of the diversity of ophiolites. Contrib. Mineral. Petrol. 89, 155–167.
Ishiwatari, A., Tsujimori, T., 2003. Paleozoic ophiolites and blueschists in Japan and Russian Primorye in the tectonic framework of East Asia: a synthesis. Island Arc 12, 190–206.
Jahn, B.M., 2004. The central Asian orogenic belt and growth of the continental crust in the phanerozoic. Geol. Soc. Spec. Publ. 226, 73–100.
Jahn, B.M., 2010. Accretionary orogen and evolution of the Japanese Islands—implications from a Sr–Nd isotopic study of the phanerozoic Granitoids from SW Japan. Am. J. Sci. 310, 1210–1249.
Jian, P., Liu, D.Y., Kroner, A., Zhang, Q., Wang, Y.Z., Sun, X.M., Zhang, W., 2009. Devonian to Permian plate tectonic cycle of the Paleo-Tethys Orogen in southwest China (I): geochemistry of ophiolites, arc/back-arc assemblages and within-plate igneous rocks. Lithos 113, 748–766.
Jian, P., Liu, D.Y., Kroner, A., Windley, B.F., Shi, Y.R., Zhang, W., Zhang, F.Q., Miao, L.C., Zhang, L.Q., Tomurhuu, D., 2010. Evolution of a Permian intraoceanic arc-trench system in the Solonker suture zone, Central Asian Orogenic Belt, China and Mongolia. Lithos 118, 169–190.
Kemkin, I.V., 2012. Microfaunal biostratigraphy and structural framework of the Nadanhada-Bikin terrane within a Jurassic accretionary prism of the Sikhote-Alin Fold Belt, eastern Russia. J. Asian Earth Sci. 61, 88–101.
Lapierre, H., Charvet, J., Blein, O., Rouer, O., 1994. The Permian–Triassic are sequences of Northwestern Nevada (USA)—key elements in the geodynamic evolution of the Cordilleran. Bull. Soc. Geol. Fr. 165, 541–557.
Lawver, L.A., Dalziel, I.W.D., Norton, I.O., Gahagan, L.M., 2009. The PLATES 2009 Atlas of Plate Reconstructions (750 Ma to Present Day). PLATES Progress Report No. 325-0509. University of Texas Technical Report No. 196, p. 52.
Lehmann, J., Schulmann, K., Lexa, O., Corsini, M., Kroner, A., Stipska, P., Tomurhuu, D., Otgonbator, D., 2010. Structural constraints on the evolution of the Central Asian Orogenic Belt in SW Mongolia. Am. J. Sci. 310, 575–628.
Li, J.Y., 2006. Permian geodynamic setting of Northeast China and adjacent regions: closure of the Paleo-Asian Ocean and subduction of the Paleo-Pacific Plate. J. Asian Earth Sci. 26, 207–224.
Li, N., 2008. Brachiopod fauna of Early Devonian Heitai Formation in Baoqing area, Heilongjiang Province and its palaeobiogeography (Master's Thesis) Jilin University.
Li, Z.X., Li, X.H., 2007. Formation of the 1300-km-wide intracontinental orogen and postorogenic magmatic province in Mesozoic South China: A flat-slab subduction model. Geology 35, 179–182.
Li, W.K., Han, J.X., Zhang, S.X., Meng, F.Y., 1979. The main characteristics of the Upper Paleozoic stratigraphy at the north Nadanhada Range, Heilongjiang Province (in Chinese with English abstract), China. Bull. Chin. Acad. Geol. Sci. 1, 104–120.
Li, H.Y., He, B., Xu, Y.G., Huang, X.L., 2010. U–Pb and Hf isotope analyses of detrital zircons from Late Paleozoic sediments: insights into interactions of the North China Craton with surrounding plates. J. Asian Earth Sci. 39, 335–346.
Li, X.H., Li, Z.X., He, B., Li, W.X., Li, Q.L., Gao, Y.Y., Wang, X.C., 2012a. The Early Permian active continental margin and crustal growth of the Cathaysia Block: in situ U–Pb, Lu–Hf and O isotope analyses of detrital zircons. Chem. Geol. 328, 195–207.
Li, Z.X., Li, X.H., Chung, S.L., Lo, C.H., Xu, X.S., Li, W.X., 2012b. Magmatic switch-on and switch-off along the South China continental margin since the Permian: transition from an Andean-type to a Western Pacific-type plate boundary. Tectonophysics 532, 271–290.
Li, K., Zhang, Z.C., Feng, Z.S., Li, J.F., Tang, W.H., Luo, Z.W., 2014a. Zircon SHRIMP U–Pb dating and its geological significance of the Late-Carboniferous to Early-Permian volcanic rocks in Bayanvvula area, the central of Inner Mongolia. Acta Petrol. Sin. 30, 2041–2054.
Li, P.F., Rosenbaum, G., Vasconcelos, P., 2014b. Chronological constraints on the Permian geodynamic evolution of eastern Australia. Tectonophysics 617, 20–30.
Liu, J.M., Zhao, Y., Sun, Y.L., Li, D.P., Liu, J., Chen, B.L., Zhang, S.H., Sun, W.D., 2010a. Recognition of the latest Permian to Early Triassic Cu–Mo mineralization on the northern margin of the North China block and its geological significance. Gondwana Res. 17, 125–134.
Liu, S., Hu, R.Z., Gao, S., Feng, C.X., Feng, G.Y., Coulson, I.M., Li, C., Wang, T., Qi, Y.Q., 2010b. Zircon U–Pb age and Sr–Nd–Hf isotope geochemistry of Permian granodiorite and associated gabbro in the Songliao Block, NE China and implications for growth of juvenile crust. Lithos 114, 423–436.
Ludwig, K.R., 2001. Squid 1.03 a user's manual. Berkeley Geochronology Center Special Publication No. 2.
Ludwig, K.R., 2003. User's Manual for Isoplot 3.0: a geochronological toolkit for Microsoft Excel. Berkeley Geochronology Center Special, Publication No.4.
Lv, D.W., Li, Z.X., Chen, J.T., Liu, H.Y., Guo, J.B., Shang, L.N., 2011. Characteristics of the Permian coal-formed gas sandstone reservoirs in Bohai Bay Basin and the adjacent areas, North China. J. Pet. Sci. Eng. 78, 516–528.
Meng, E., Xu, W.L., Yang, D.B., Pei, F.P., Yu, Y., Zhang, X.Z., 2008. Permian volcanisms in eastern and southeastern margins of the Jiamusi Massif, northeastern China: zircon U–Pb chronology, geochemistry and its tectonic implications. Chin. Sci. Bull. 53, 1231–1245.
Meng, E., Xu, W.L., Pei, F.P., Yang, D.B., Wang, F., Zhang, X.Z., 2011. Permian bimodal volcanism in the Zhangguangcai Range of eastern Heilongjiang Province, NE China: zircon U–Pb–Hf isotopes and geochemical evidence. J. Asian Earth Sci. 41, 119–132.
Mizutani, S., Kojima, S., 1992. Mesozoic Radiolarian Biostratigraphy of Japan and Collage Tectonics Along the Eastern Continental-Margin of Asia. Palaeogeogr. Palaeoclimatol. Palaeoecol. 96, 3–22.
Mizutani, S., Shao, J., Zhang, Q.L., 1990. The Nadanhada Terrane in relation to mesozoic tectonics on continental margins of East-Asia. Acta Geol. Sin. Engl. 3 (1), 15–29.
Mullen, E.D., 1983. MnO/TiO2/P2O5—a minor element discriminant for basaltic rocks of oceanic environments and its implications for petrogenesis. Earth Planet. Sci. Lett. 62, 53–62.
Nelson, D.R., Myers, J.S., Nutman, A.P., 1995. Chronology and evolution of the Middle Proterozoic Albany-Fraser Orogen, Western-Australia. Aust. J. Earth Sci. 42, 481–495.
Pearce, J.A., 2014. Immobile element fingerprinting of ophiolites. Elements 10, 101–108.
Pearce, T.H., Gorman, B.E., Birkett, T.C., 1975. TiO2–K2O–P2O5 diagram—method of discriminating between oceanic and non-oceanic basalts. Earth Planet. Sci. Lett. 24, 419–426.
Phillips, G., Offler, R., 2011. Contrasting modes of eclogite and blueschist exhumation in a retreating subduction system: the Tasmanides, Australia. Gondwana Res. 19, 800–811.
Rosenbaum, G., Li, P.F., Rubatto, D., 2012. The contorted New England Orogen (eastern Australia): new evidence from U–Pb geochronology of early Permian granitoids. Tectonics 31.
Rouer, O., Lapierre, H., Coulon, C., 1988. The Permian Calc–Alkaline Island–Arc Suite of Northern Sierra-Nevada—magmatic final stage on the Sonomia microplate. C. R. Acad. Sci. II 307, 57–62.
Sano, S., 1992. Neodymium isotopic compositions of Silurian Yakuno metagabbros. J. Mineral. Petrol. Econ. Geol. 87, 272–282.
Shao, J.A., Tang, K.D., Wang, C.Y., Zang, Q.J., Zhang, Y.P., 1992. Structural features and evolution of the Nadanhada Terrane. Sci. China B 35 (5), 621–630.
Shervais, J.W., 1982. Ti–V plots and the petrogenesis of modern and ophiolitic lavas. Earth Planet. Sci. Lett. 59, 101–118.
Sivell, W.J., McCulloch, M.T., 2001. Geochemical and Nd-isotopic systematics of the Permo-Triassic Gympie Group, southeast Queensland. Aust. J. Earth Sci. 48, 377–393.
Sivell, W.J., Waterhouse, J.B., 1988. Petrogenesis of Gympie Group Volcanics—evidence for remnants of an early Permian volcanic arc in Eastern Australia. Lithos 21, 81–95.
Soderlund, U., Patchett, J.P., Vervoort, J.D., Isachsen, C.E., 2004. The Lu-176 decay constant determined by Lu–Hf and U–Pb isotope systematics of Precambrian mafic intrusions. Earth Planet. Sci. Lett. 219 (3-4), 311–324.
Sorokin, A.A., Kotov, A.B., Sal'nikova, E.B., Kudryashov, N.M., Anisimova, I.V., Yakovleva, S.Z., Fedoseenko, A.M., 2010. Granitoids of the Tyrma–Bureya complex in the northern Bureya–Jiamusi superterrane of the Central Asian fold belt: age and geodynamic setting. Russ. Geol. Geophys. 51, 563–571.
Spandler, C., Worden, K., Arculus, R., Eggins, S., 2005. Igneous rocks of the Brook Street Terrane, New Zealand: implications for Permian tectonics of eastern Gondwana and magma genesis in modern intra-oceanic volcanic arcs. New. Zeal. J. Geol. Geop. 48, 167–183.
Stern, R.A., 2001. A New Isotopic and Trace-Element Standard for the Ion Microprobe: Preliminary Thermal Ionization Mass Spectrometry (TIMS) U–Pb and Electron-Microprobe Data. Ressources Naturelles Canada.
Suda, Y., Hayasaka, Y., 2009. Genesis and evolutional processes of the Paleozoic oceanic island arc crust, Asago body of the Yakuno Ophiolite, Southwest Japan. J. Geol. Soc. Jpn. 115, 266–287.

Suda, Y., Hayasaka, Y., Kimura, K., 2014. Crustal evolution of a Paleozoic intra-oceanic island-arc–back-arc basin system constrained by the geochemistry and geochronology of the Yakuno Ophiolite, Southwest Japan. J. Geophys. Res. 2014, 10.
Sun, S.S., McDonough, W.F., 1989. Chemical and isotopic systematics of oceanic basalts: implications for mantle composition and processes. In: Saunders, A.D., Norry, M.J. (Eds.), Magmatism in the Ocean Basins. Geological Society Special Publication, London, pp. 313–345.
Sun, M.D., Xu, Y.G., Wilde, S.A., Chen, H.L., 2015. Provenance of Cretaceous trench slope sediments from the Mesozoic Wandashan Orogen, NE China: Implications for determining ancient drainage systems and tectonics of the Paleo-Pacific. Tectonics 34, 1269–1289.
Ueno, K., 2003. The Permian fusulinoidean faunas of the Sibumasu and Baoshan blocks: their implications for the paleogeographic and paleoclimatologic reconstruction of the Cimmerian Continent. Palaeogeogr. Palaeoclimatol. Palaeoecol. 193, 1–24.
Vervoort, J.D., Plank, T., Prytulak, J., 2011. The Hf-Nd isotopic composition of marine sediments. Geochim. Cosmochim. Acta 75, 5903–5926.
Wakita, K., 2013. Geology and tectonics of Japanese islands: a review—the key to understanding the geology of Asia. J. Asian Earth Sci. 72, 75–87.
Wan, Y.S., Li, R.W., Wilde, S.A., Liu, D.Y., Chen, Z.Y., Yan, L., Song, T.R., Yin, X.Y., 2005. UHP metamorphism and exhumation of the Dabie Orogen, China: evidence from SHRIMP dating of zircon and monazite from a UHP granitic gneiss cobble from the Hefei Basin. Geochim. Cosmochim. Acta 69 (17), 4333–4348.
Wang, F., Xu, W.-L., Xu, Y.-G., Gao, F.-h., Ge, W.-c., 2015. Late Triassic bimodal igneous rocks in eastern Heilongjiang Province, NE China: implications for the initiation of subduction of the Paleo-Pacific Plate beneath Eurasia. J. Asian Earth Sci. 97 (Part B), 406–423.
Wilde, S.A., Zhou, J.-B., 2015. The late Paleozoic to Mesozoic evolution of the eastern margin of the Central Asian Orogenic Belt in China. J. Asian Earth Sci. http://dx.doi.org/10.1016/j.jseaes.2015.05.005 (In press).
Wilde, S.A., Dorsett-Bain, H.L., Lennon, R.G., 1999. Geological setting and controls on the development of graphite, sillimanite and phosphate mineralization within the Jiamusi Massif: an exotic fragment of Gondwanaland located in north-eastern China? Gondwana Res. 2, 21–46.
Wilde, S.A., Zhang, X.Z., Wu, F.Y., 2000. Extension of a newly identified 500 Ma metamorphic terrane in North East China: further U–Pb SHRIMP dating of the Mashan Complex, Heilongjiang Province, China. Tectonophysics 328, 115–130.
Windley, B.F., Alexeiev, D., Xiao, W.J., Kroner, A., Badarch, G., 2007. Tectonic models for accretion of the Central Asian Orogenic Belt. J. Geol. Soc. Lond. 164, 31–47.
Wood, D.A., 1980. The Application of a Th–Hf–Ta Diagram to Problems of Tectonomagmatic Classification and to Establishing the Nature of Crustal Contamination of Basaltic Lavas of the British Tertiary Volcanic Province. Earth Planet. Sci. Lett. 50, 11–30.
Wu, F.Y., Wilde, S., Sun, D.Y., 2001. Zircon SHRIMP U–Pb ages of gneissic granites in Jiamusi massif, northeastern China. Acta Petrol. Sin. 17, 443–452.
Wu, F.Y., Sun, D.Y., Ge, W.C., Zhang, Y.B., Grant, M.L., Wilde, S.A., Jahn, B.M., 2011. Geochronology of the Phanerozoic granitoids in northeastern China. J. Asian Earth Sci. 41, 1–30.
Xiao, W.J., Windley, B.F., Hao, J., Zhai, M.G., 2003. Accretion leading to collision and the Permian Solonker suture, Inner Mongolia, China: termination of the central Asian orogenic belt. Tectonics 22.
Xiao, W.J., Windley, B.F., Sun, S., Li, J.L., Huang, B.C., Han, C.M., Yuan, C., Sun, M., Chen, H.L., 2015. A tale of amalgamation of three permo-triassic collage systems in central Asia: oroclines, sutures, and terminal accretion. Annu. Rev. Earth Planet. Sci. 43, 477–507.
Xu, W.L., Ji, W.Q., Pei, F.P., Meng, E., Yu, Y., Yang, D.B., Zhang, X.Z., 2009. Triassic volcanism in eastern Heilongjiang and Jilin provinces, NE China: chronology, geochemistry, and tectonic implications. J. Asian Earth Sci. 34, 392–402.
Yang, M.H., Liu, C.Y., Lan, C.L., Liu, L., Li, X., Zhang, K.S., 2010. Late Carboniferous-Early Permian Sequence Stratigraphy and Depositional Evolution in the Northeast Ordos Basin, North China. Acta Geol. Sin. Engl. 84, 1220–1228.
Yang, H., Ge, W.C., Zhao, G.C., Yu, J.J., Zhang, Y.L., 2015. Early Permian-Late Triassic granitic magmatism in the Jiamusi-Khanka Massif, eastern segment of the Central Asian Orogenic Belt and its implications. Gondwana Res 27, 1509–1533.
Yu, J.H., Liu, Q., Hu, X.M., Wang, Q., O'Reilly, S.Y., 2013a. Late Paleozoic magmatism in South China: oceanic subduction or intracontinental orogeny? Chin. Sci. Bull. 58, 788–795.
Yu, J.J., Hou, X.G., Ge, W.C., Zhang, Y.L., Liu, J.C., 2013b. Magma mixing genesis of the Early Permian Liulian pluton at the northeastern margin of the Jiamusi massif in NE China: evidence from petrography, geochronology and geochemistry. Acta Petrol. Sin. 29, 2971–2986.
Zhang, K.W., Shao, J.A., Tang, K.D., Zhang, Q., Li, X.Y., 1997. The geochemical characteristics and the geological significance of green schists in Yuejinshan Group, East Heilongjiang Province, China. Acta Petrol. Sin. 13, 168–172.
Zhang, S.H., Zhao, Y., Song, B., Hu, J.M., Liu, S.W., Yang, Y.H., Chen, F.K., Liu, X.M., Liu, J., 2009. Contrasting Late Carboniferous and Late Permian–Middle Triassic intrusive suites from the northern margin of the North China craton: geochronology, petrogenesis, and tectonic implications. Geol. Soc. Am. Bull. 121, 181–200.
Zhao, P., Chen, Y., Xu, B., Faure, M., Shi, G.Z., Choulet, F., 2013. Did the Paleo-Asian Ocean between North China Block and Mongolia Block exist during the late Paleozoic? First paleomagnetic evidence from central-eastern Inner Mongolia, China. J. Geophys. Res. Solid Earth 118, 1873–1894.
Zhong, Y.T., He, B., Xu, Y.G., 2013. Mineralogy and geochemistry of claystones from the Guadalupian-Lopingian boundary at Penglaitan, South China: insights into the pre-Lopingian geological events. J. Asian Earth Sci. 62, 438–462.
Zhou, J.B., Wilde, S.A., 2013. The crustal accretion history and tectonic evolution of the NE China segment of the Central Asian Orogenic Belt. Gondwana Res. 23, 1365–1377.
Zhou, X.M., Sun, T., Shen, W.Z., Shu, L.S., Niu, Y.L., 2006. Petrogenesis of Mesozoic granitoids and volcanic rocks in South China: a response to tectonic evolution. Episodes 29, 26–33.
Zhou, J.B., Wilde, S.A., Zhang, X.Z., Zhao, G.C., Zheng, C.Q., Wang, Y.J., Zhang, X.H., 2009. The onset of Pacific margin accretion in NE China: evidence from the Heilongjiang high-pressure metamorphic belt. Tectonophysics 478, 230–246.
Zhou, J.B., Wilde, S.A., Zhao, G.C., Zhang, X.Z., Zheng, C.Q., Wang, H., Zeng, W.S., 2010. Pan-African metamorphic and magmatic rocks of the Khanka Massif, NE China: further evidence regarding their affinity. Geol. Mag. 147, 737–749.
Zhou, J.B., Cao, J.L., Wilde, S.A., Zhao, G.C., Zhang, J.J., Wang, B., 2014. Paleo-Pacific subduction-accretion: Evidence from Geochemical and U–Pb zircon dating of the Nadanhada accretionary complex, NE China. Tectonics 33, 2444–2466.